2009-01-01

Insight Into The Physics Of Rupture: Dynamic Triggering Seismicity

Hector Gonzalez-Huizar
University of Texas at El Paso, hectorg@miners.utep.edu

INSIGHT INTO THE PHYSICS OF RUPTURE:

DYNAMIC TRIGGERING SEISMICITY

HECTOR GONZALEZ-HUIZAR

Department of Geological Sciences

APPOVED:

_____
Aaron A. Velasco, Ph.D. Chair

_____
Diane I. Doser, Ph.D.

_____
Jose Hurtado, Ph.D.

_____
Winston Lloyd, Ph.D.

_____
Bridget Smith-Konter, Ph.D.

_____
Patricia D. Witherspoon, Ph.D.
Dean of the Graduate School

INSIGHT INTO THE PHYSICS OF RUPTURE:

DYNAMIC TRIGGERING SEISMICITY

by

HECTOR GONZALEZ-HUIZAR

DISSERTATION

Presented to the Faculty of the Graduate School of

The University of Texas at El Paso

in Partial Fulfillment

of the Requirements

for the Degree of

DOCTOR OF PHILOSOPHY

Department of Geological Sciences

THE UNIVERSITY OF TEXAS AT EL PASO

August 2009

ACKNOWLEDGMENTS

All my appreciation goes to my wife Claudia for her love and support and for my son Gael Isaac, thank you both for been my inspiration.

I would like to express my sincere appreciation to Dr. Aaron Velasco for his supervision and advice during the progress of this work.

Many greetings go to the graduate committee Dr. Diane I. Doser, Dr. Jose Hurtado, Dr. Bridget Simth-Konter and Dr. Winston Lloyd for their advice.

Thanks to all my family members and friends.

Thanks to God!

ABSTRACT

Seismic waves can trigger earthquakes and tremor at large distances from the causable event. Dynamic triggering occurs when the surface waves from large earthquakes change the stresses conditions on previously overstressed faults, promoting failure. To understand the causative stresses and environments behind dynamic triggering, we model the change in the stress field that the passing of Rayleigh and Love waves cause on a fault plane of arbitrary orientation relative to the direction of propagation of the waves, and apply a Coulomb failure criterion to calculate the potential of these stress changes to trigger seismicity. We apply our model to three different study regions and compare with observations. In the first case, we compare our model results with data from dynamically triggered earthquakes in the Australian Bowen Basin, Our data analysis shows that for this region, surface waves arriving at 45 degrees from the average local stress field are the most likely to trigger local seismicity. This agrees with our observations. In the second study case, we show how the same model can be applied to dynamic triggering of Non-volcanic tremor (NVT). Our modeling predicts the potential of a seismic wave to trigger slip on a fault plane promoting NVT. We search for tremor in the Central Range in Taiwan triggered by surfaces waves and compare the observations with our modeling. In the last study case, we present our modeling of the dynamic stress that triggered two events in Utah, one triggered by the 1992 Landers earthquake and the other by the 2002 Denali Fault earthquake. We show how dynamic stress modeling can be used to discriminate between the two axial planes of a first motion focal mechanism of a dynamically triggered event.

TABLE OF CONTENTS

Page

CHAPTER 1

INTRODUCTION

Recent studies have shown that seismic waves can remotely trigger seismicity thousands of kilometers from an epicenter. This process is called dynamic. This dissertation focus on the modeling of the dynamic stress caused by the passing of the surface waves from large earthquakes and their potentials to trigger seismicity base on the characteristics of the waves, the position and orientation of the triggered fault plane and the elastic properties of the media.

Dynamic triggering has been clearly documented for several large earthquakes including the 1992 Landers (M_w = 7.3) (Hill et al., 1993; Anderson et al., 1994;), the 2002 Denali Fault (M_w = 7.9) (Eberhart-Phillips et al., 2003; Gomberg et al., 2004; Husen and Wiemer, 2004; Pankow et al, 2004; Prejean et al., 2004), and the 2004 Sumatra (M_w = 9.15) (West et al., 2005; Velasco et al., 2008) earthquakes. Many studies on dynamic triggering seismicity focus on the triggering of small earthquakes on previously overstressed faults (e.g., Velasco et al., 2008). Recent studies have also demonstrate that non-volcanic tremor (NVT) can be triggered by seismic waves as well (Obara, 2002; Nadeau and Dolec et al., 2005; Miyazawa and Mori, 2006; Rubinstein et al., 2007; Gomberg et al., 2004; Miyazawa and Brosky 2008; Peng et al., 2008; Peng and Chao, 2008). NVT is usually observed in subduction zone and transform-fault environments away from volcanic regions. We apply our modeling to the triggering of earthquakes and NVT, and compare our model result with observations.

Dynamic triggering may occur when surface waves passing through a previously overstressed fault plane change the fault local stress in a suitable manner. Our modeling allows

for the calculation of the dynamic contributions to the shear and normal stresses on a fault plane of arbitrary orientation. In Chapter 2 we develop the modeling and show and compare it with observations from triggered seismicity in the Australian Bowen region. We found that for this region, seismicity is more likely to be triggered by Love waves arriving at 45º from the average local compressive stress orientation. Observed events similar to those predicted by the modeled potentials demonstrate that our model suitably represents the stress caused by the passing of the surface waves and that dynamic triggering seismicity can be explained on Coulomb stress basis.

In Chapter 3, we show that dynamic triggering of NVT can be modeled based on the same Coulomb frictional approach. We identified three large events besides the 2001 Kunlun earthquakes that have had triggered NVT beneath the CR in Taiwan: The 2003 Hokkaido, the 2004 Sumatra, and the 2005 Sumatra earthquakes. We modeled the stress caused by the surface waves from ten large earthquakes to investigate the stress conditions required to trigger NVT in this region. For the Kunlun earthquake, our modeling shows that the orientation and magnitude of the incoming Love wave contributes to increasing the fault plane local shear stress. In the cases of the Hokkaido and Sumatra earthquakes, the orientation and magnitude of the incoming Rayleigh waves contribute to the shear local stress. In general, NVT correlates with peaks in our modeled triggering potential.

In Chapter 4 we analyzed the dynamic stress caused by the passing of the surfaces waves from two large events, the 1992 Landers earthquake and the 2002 DFE that triggered seismicity in Utah. We modeled the stress that triggered two of the largest dynamically triggered events in this region, both of which show a well-constrained normal fault mechanism. We showed how dynamic stress modeling can be used to discriminate between the axial planes of a first motion focal mechanism of a dynamically triggered event.

The modeling of dynamic stress triggering constitutes an important tool for understanding the stress conditions under which earthquakes occur. The study of the local static–dynamic stress interaction will lead to a better understanding of the fault cycle, and at some point, dynamic triggering events could be used as a regional local stress indicator.

CHAPTER 2

DYNAMIC TRIGGERING: STRESS MODELING AND A CASE STUDY

2.1 ABSTRACT

Changes in the static stress can trigger nearby earthquakes that occur within a few fault lengths from the causative event. Transient stresses caused by passage of surface waves commonly trigger events at remote distances, yet little is documented or understood about the processes and stresses necessary for remote triggering. To understand the causative stresses and environments behind remote, or dynamic, triggering, we must decipher the stresses caused by the passage of the surface waves in relation to the local stress field and fault conditions where the triggered events occur. In this study, we model the change in the stress field that the passing of Rayleigh and Love waves cause on a fault plane of arbitrary orientation relative to the direction of propagation of the waves, and apply a Coulomb failure criterion to calculate the potential of these stress changes to trigger reverse, normal or strike-slip failure. We compare these model results with data from dynamically triggered earthquakes in the Australian Bowen Basin, an area with low seismicity, mapped regional stress, and at the margin of a stable continental craton. Our data analysis shows that for this region, surface waves arriving at 45 degrees from the average local stress field are the most likely to trigger local seismicity. This agrees with our observations.

2.2 INTRODUCTION

Although our understanding of earthquakes and faulting has grown tremendously since the development of Elastic Rebound Theory (Reid, 1910), many questions remain about the

fundamental physics behind earthquake rupture. Some questions stem from a growing body of works that shows that the passage of transient signals, such as seismic waves, can remotely trigger earthquakes thousands of kilometers from an epicenter. This process is called dynamic triggering. Generally, dynamic triggering results from the passage of surface waves, which are classified by two distinct types: Rayleigh and Love. Rayleigh waves exhibit shearing and compressional, dilatational, and shear particle motion. Love waves only induce shearing. Triggering by either type of surface waves implies fundamentally different physical mechanisms. The first accepted case that dynamic triggering occurred was documented for the 1992 Landers (M_w = 7.3) event (Hill et al., 1993; Anderson et al., 1994). Dynamic triggering has subsequently been shown to have occurred for the 2002 Denali event (M_w = 7.9) (Eberhart-Phillips et al., 2003; Gomberg et al., 2004; Husen and Smith, 2004; Pankow et al., 2004; Prejean et al, 2004), and the 2004 Sumatra event (M_w = 9.15) (West et al., 2005; Velasco et al., 2008) earthquakes. Velasco et al. (2008) studied 15 large events and showed that 12 of them had some evidence of dynamic triggering and their occurrence was virtually independent of tectonic province.

Mechanisms for dynamic triggering fall into two broad categories (Hill, 2008; Prejean et al., 2007): (1) Models related to the excitation of crustal fluids or aseismic creep or (2) frictional models described by Coulomb failure. Most of the studies focusing on the physical processes of dynamic triggering are associated with geothermal activity, such as the movement of magmatic fluids, magmatic intrusions, or bubble excitation (Hill et al., 1993; Linde et al., 1998). Other examples of proposed mechanisms include subcritical crack growth that is accelerated by seismic waves (Brodsky et al., 2000), pore fluid flow along with Coulomb stress changes (e.g., Bosl and Nur, 2002), and unclogging of fractures (Brodsky et al., 2003). A similar mechanism is that fluid flow acts as a low pass filter for seismic waves (Brodsky and Prejean, 2005). This mechanism

predicts that long period waves lead to high-pressure oscillations. Alternatively, rate-and-state friction has been proposed to cause dynamic triggering of earthquakes (e.g. Dieterich et al., 1994; Gomberg et al., 2001; Perfettini et al, 2003). Perfettini et al. (2003), used a 2-D quasi-dynamic model of a strike-slip fault, governed by a rate-and-state friction law, to show that dynamic triggering is limited to understressed areas, that is, areas of high pore pressure or faults near failure. Brodsky and Prejean et al. (2005) found similar results by analyzing triggered earthquakes predicted by the rate- and state-model. Parsons (2005) showed that in the presence of rate- and state-friction, if the passing seismic waves 'damage' the fault contacts, dynamic triggering could explain both delayed earthquakes and the Omori-like decay of triggered earthquakes. Hill et al. (2008) developed a Coulomb failure model based on a frictional strength threshold using Mohr's Circle, yet the model cannot fully explain the dominance of documented Rayleigh wave triggering. Although fluids appear in many dynamic triggering explanations, West et al. (2005) demonstrated that at Mt. Wrangell, Alaska, the fluid effect is a secondary factor. Dynamic triggering at Mt. Wrangell was primarily attributed to changes in horizontal normal stresses. This is similar to the mechanisms proposed by Brune et al. (1993) and Anderson et al. (1994) who suggested that triggered earthquakes are caused by unclamping of faults that are in a preferred orientation relative to the passing seismic waves. The multitude of explanations for dynamic triggering suggests that this process is poorly understood and severely lacking in extensive study and modeling.

In this paper, we build upon the results of Hill et al. (2008) who presented an analysis of the dynamic stresses associated with fundamental-mode Love and Rayleigh waves and their potentials to trigger frictional failure on critically stressed faults. However, Hill et al.'s (2008) study is limited to faults of specific orientations. In this article, we present a method for

modeling triggering potentials, but for an arbitrary fault plane orientation relative to the direction of the triggering wave propagation. In addition, we analyze the likelihood of the faults to be triggered by the different parts of a wave cycle over time. We present an example of dynamically triggered seismicity in the Australian Bowen Basin, an area with mapped regional stress, low seismicity, and at the margin of a stable continental craton. Our results show that Love waves arriving at 45º from the principal stress axis of faults present in this region are the most likely to trigger local seismicity which supports the idea that passing seismic waves unclamp faults.

2.3 COULOMB STRESS FAILURE CRITERIA

Dynamic triggering may occur when surface waves pass through a previously overstressed fault plane and change the fault local stress in a suitable manner. If τ and σ_n represent the changes caused by the passing of the triggering seismic waves on the fault plane's shear and normal stresses, respectively, according to the Coulomb Failure Criteria, the fault will be brought closer to failure if the change in the Coulomb Failure Function δCFF defined as:

$$\delta CFF = \tau + \mu\sigma_n \tag{2.1}$$

. where μ is the coefficient of friction. If δCFF is positive, or it will be moved away from failure if δCFF is negative. To calculate the components of the dynamic stress tensor that correspond to the shear and normal directions of a fault plane of arbitrary orientation as a function of depth and time, we calculate the dynamic stress tensor $T^0(D,t)$ for surface waves, as function of depth (D) and time (t), for a coordinate system with one component parallel to the direction of wave propagation and the other in the depth direction (Figure 2.1). We rotate this tensor to a new coordinate system with components parallel to the dip, strike, and normal directions of a fault

plane of arbitrary orientation (α,θ), to obtain a new tensor *T(D,t,α,θ).* We then calculate components of the fault plane's shear and normal stresses for different faulting mechanisms caused by the new tensor. We then apply the values of these stress components to equation (2.1) to estimate a triggering potential indicator (P). This is discussed and developed below in detail.

2.4 DYNAMIC STRESSES ON AN ARBITRARY FAULT PLANE

We use the technique of West et al. (2005) to model the stress change caused by the passing of Rayleigh waves. We extend this modeling to include the components of the dynamic stress tensor $T^0(D,t)$ related to the displacement of both the Rayleigh and Love waves as a function of time and depth. For a coordinate system x_i where *i* = 1, 2, 3, the Rayleigh waves' related particle displacement for a Poisson half space in the radial U_1 and vertical U_3 directions for a wave propagating in the x_1 direction is defined by (Stein and Wyssession, 2003):

$$U_1 = AK_1 \sin(wt - \kappa_1 x_1)[\exp(B\kappa_1 x_3) - C\exp(D\kappa_1 x_3)] \tag{2.2}$$

$$U_3 = AK_1 \cos(wt - \kappa_1 x_1)[B\exp(B\kappa_1 x_3) + E\exp(D\kappa_1 x_3)] \tag{2.3}$$

where *A* is amplitude, ω is the angular frequency, κ_1 is horizontal wave number, and x_3 is depth. Coefficients *B* = -0.85, *C* = 0.58, *D* = -0.39, and *E* = 1.47 are constants. Rayleigh waves do not cause motion in the U_2 direction. The strains ε_{ij} induced by the motion are given by:

$$\varepsilon_{ij} = \varepsilon_{ji} = \frac{1}{2}\left(U_{i,j} + U_{j,i}\right) \tag{2.4}$$

where $U_{i,j}$ represents the first derivative of the displacement in the *i* direction relative to the *j* direction.

In general, the components of the stress tensor are defined by:

$$\sigma_{i,j} = c_{ijkl}\varepsilon_{kl} \tag{2.5}$$

where c_{ijkl} accounts for the elastic properties of the media.

The transient stresses σ_{ij}, assuming a Poisson solid ($\mu = \lambda$), are defined by:

$$\sigma_{11} = \lambda(\varepsilon_{11} + \varepsilon_{33}) + 2\mu\varepsilon_{11} = \lambda(3\varepsilon_{11} + \varepsilon_{33}) \tag{2.6}$$

$$\sigma_{33} = \lambda(\varepsilon_{11} + \varepsilon_{11}) + 2\mu\varepsilon_{33} = \lambda(\varepsilon_{11} + 3\varepsilon_{33}) \tag{2.7}$$

$$\sigma_{13} = \sigma_{31} = 2\lambda\varepsilon_{13} \tag{2.8}$$

where normal stresses are negative for compression and positive for dilatation.

To model Love waves we consider the displacement in the transverse direction, U_2, within a layer over a half space (e.g. Stein and Wyssession et al., 2003), such that

$$U_2 = A\exp(i(wt - \kappa_1 x_1))\cos(K_1 r_\beta x_3) \tag{2.9}$$

where A is the amplitude and κ_1 is the transverse displacement component's wave number and

$$r_\beta = \left(\frac{c_1^2}{\beta_1^2} - 1\right)^{\frac{1}{2}} \tag{2.10}$$

where c_1 is the surface wave's apparent velocity and β_1 is the shear velocity for the layer. The related shear strains ε_{ij} are calculated using equation (2.4). The shear stress components for Love waves are:

$$\sigma_{12} = \sigma_{21} = 2\mu\varepsilon_{12} \tag{2.11}$$

$$\sigma_{23} = \sigma_{32} = 2\mu\varepsilon_{23} \tag{2.12}$$

Figure 2.2 shows the dynamic stresses as function of time and depth produced by a 20-s period Rayleigh wave and a 20-s period Love wave. This kind of modeling allows us to determine what components of the stress tensor play an important role in the triggering of a fault

located at a given depth, and at a given moment in time. For normal stresses, the red color represents dilatation and blue compression, whereas for shear stress the color defines the direction of the shearing. The change over time of the directions and magnitudes of the stress components occurs in phase with the ground displacement at the surface. Figure 2.2 also shows how stress depends on depth. For example, at shallow depths, Rayleigh wave's normal stresses and Love waves horizontal shear stress mainly act on planes perpendicular to the direction of wave propagation (σ_{11} and σ_{21} reach a maximum at surfaces). However, at greater depths, normal stress and lateral shearing is stronger on horizontal planes (σ_{33} and σ_{23} increase with depth). Also note that the shear stress caused by Rayleigh waves (σ_{13}) increases with depth. This dependency of the stress components on depth, in general, is a function of the frequency of the waves.

Our next step is to model the effects of these stresses on fault planes of arbitrary orientation. The components of the dynamic stress acting on a plane of arbitrary orientation can be calculated by rotating the stress tensor $T^0(D,t)$ (Figure 2.1). By multiplying $T^0(D,t)$ by the matrices of the Euler angles (Arfken, 1995), we can rotate to the fault plane orientation around the angles (α, θ) relative to the direction of propagation, as defined in Figure 1, to obtain a new matrix *T(D,t,α,θ)* corresponding to stresses on the rotated plane. We define $\delta\sigma_n(\theta,\alpha)$, $\delta\tau_d(\theta,\alpha)$, and $\delta\tau_s(\theta,\alpha)$ as the components of *T(D,t,α,θ)* acting in the normal, dip, and strike direction of the fault plane, respectively (Figure 2.1). Figure 2.3 shows the stress that the passing of a Love wave similar to that of Figure 2.2 will cause on a plane of arbitrary orientation at a depth of 5 km and time equal to 5 s. Note that even though the Love wave causes only shear stresses on a coordinate system with one component in the direction of propagation and the other

in the depth direction, Love waves will cause a change in the normal stress ($\delta\sigma_n$) on a rotated planes, reaching a maximum value for vertical planes (θ = 90 º) striking 45º (α = 45º) from the direction of propagation. In this fashion, we can model the change in local stress that passing surface waves will cause on a fault plane of arbitrary orientation. The next step is to calculate if this change will promote faulting.

2.5 TRIGGERING POTENTIAL

We define the triggering potential *P* of a seismic wave as the change of the Coulomb failure function (equation 2.1) that the passing of the seismic wave causes on a fault plane. The definition of the potentials will depend on the kind of faulting mechanism that is been triggered. Potential is positive if failure is encouraged and negative if discouraged. For example, $\delta\tau_d$ represents a change in the fault plane's shear stress in the dip direction, where a positive value represents a contribution in the reverse direction. Consequently, when defining the potential for a reverse fault the shear stress in equation (2.1) will be represented by $+\delta\tau_d$ whereas for a normal fault, it will be $-\delta\tau_d$ so that a negative value of $\delta\tau_d$, meaning a contribution in the normal direction, will make *P(Reverse)* more negative and *P(Normal)* more positive. On the other hand, a positive value of $\delta\sigma_n$ indicates that the fault is unclamped, encouraging failure. Hence, all cases $+\delta\sigma_n$ will represent the change in the fault normal stress. In the same way, the potentials of triggering strike-slip faults are defined below, where the change in shear stress will be in the strike direction ($\delta\tau_s$).

$$P \text{ (Reverse)} = \delta\tau_d + \mu\delta\sigma_n \tag{2.13}$$

$$P \text{ (Normal)} = -\delta\tau_d + \mu\delta\sigma_n \quad (2.14)$$

$$P \text{ (Strike-slip Left-lateral)} = \delta\tau_s + \mu\delta\sigma_n \quad (2.15)$$

$$P \text{ (Strike-slip Right-lateral)} = -\delta\tau_s + \mu\delta\sigma_n \quad (2.16)$$

In general these potentials are a function of time, depth, wave characteristics (frequency, velocity and amplitude), and elastic properties of the media. We calculate the potential, $P(D, t, \alpha, \theta)$ for surface waves as a function of time (t) to trigger failure on a normal, reverse or strike-slip fault plane of arbitrary depth D, and orientation (α, θ) (Figure 2.1). Figure 2.4 shows an example of the potentials using the values in Figure 2.3, corresponding to a Love wave when time equals 5 s (Figure 2.2). Under these conditions, the maximum value of P is reached for strike-slip right-lateral faulting, specifically, for vertical faults ($\theta = 90°$) with a 70° angle (α) with the direction of wave propagation, meaning that this type of fault motion is most likely to be triggered by this specific wave.

This kind of analysis provides us with an important tool for understanding the stress conditions under which failure occurs. By modeling stress changes associated with the Love and Rayleigh we can understand why a particular wave is more likely to trigger a specific kind of earthquake mechanism, and why triggering occurs at a specific moment in time. For example, Figure 2.5 shows the potentials for four key points of the both a 20-s period Love and a 20-s period Rayleigh waves: the negative- and positive-slope inflexion points, and for the maximum and minimum displacements. With our modeling we can estimate the type of faulting mechanism and/or fault orientation that is the most likely to be triggered by the Love or Rayleigh wave as a function of time and depth. This modeling can also help us to identify what part of the wave is responsible for triggering of a known fault (type and orientation) relative to the direction of wave

propagation. To test our model, we focus on a region with documented dynamic triggering, a regional with mapped local stress field, and that is not near a major tectonic boundary.

2.6 CASE STUDY: DYNAMIC TRIGGERING IN THE AUSTRALIAN BOWEN REGION

Velasco et al. (2008) showed the abundance of dynamic triggering that occurs with the passage of surface waves from large earthquakes. They showed that dynamic triggering can occur in areas that are not thought to be tectonically active, and they suggest that triggering is a process independent of tectonic setting. To further investigate this result, we focus on an area that showed dynamic triggering in their study, the Australian Bowen Region (Figure 2.6) an area with relatively low seismicity (Leonard et al., 2008), located at the margin of a stable continental craton. We analyzed seismograms from large, and we apply a high-pass filter to identify small local earthquakes hidden in the broadband spectrum of surfaces waves (Figure 2.7). We used stress data for this region (Hillis et al., 1998; Hillis et al., 1999) in order to compare observed dynamic triggering to local stress field orientations, and in the process, test our modeling results.

Reverse faults are mainly present in the Bowen Basin (Hillis et al., 1999). We know the faults have an average dip angle and of 70º and 340º, respectively. Assuming that triggering occurred along some of these reverse faults, we can isolate from Figure 2.5 the potential corresponding to reverse faulting and $\theta = 70^{o}$ (Figure 2.8 and 2.9). Figures 2.8 and 2.9 shows the potentials extracted from Figure 2.5 for the Rayleigh and Love waves, respectively, as a function of incident angle α and time. We can see that for Rayleigh waves (Figure 2.8) maximum potential is reached at the negative inflection point in the vertical displacement (first panel from left to right), The maximum potential occurs for waves arriving perpendicularly to the strike of the fault planes ($\alpha = 0^{o}$). The polar diagram shows the overall potential (for the whole wave cycle) as function of α, once again showing that Rayleigh waves arriving perpendicular to the

strike of the fault planes are the most likely to trigger seismicity. Figure 2.9 shows that a maximum potential of the Love waves occurs at the inflection points, where waves arrive at 45º from the fault strike. Note that maximum potential for Love waves is almost double that for Rayleigh waves, indicating that Love waves are the most likely to trigger seismicity in the Bowen region. Figure 10 overlaps the Love and Rayleigh potentials and shows their relation with the average local compressive stress for reverse faulting. Our model predicts that Love waves arriving at 45º from the local compressive stress are the most likely to trigger seismicity in the Bowen region (Figure 2.10).

To test our prediction (Figure 2.10), we performed a search for dynamically triggered earthquakes recorded near the Bowen region. We looked for triggered local seismicity caused by passing surfaces waves produced by large ($M_w \geq 7.0$) earthquakes that occurred since 1992. We obtained three component broadband seismograms from IRIS (Incorporated Research Institutions in Seismology) for the CTAO.IU station (Figure 2.6) for 5 hours before and 5 hours after the origin times of the large events. For this analysis, we manually identified small, local events from the high pass filtered traces. Figure 2.7 shows an example of the identification of a dynamic triggered event caused by the March 1998 Balleny Island earthquake. In our data set, 8 out of 35 large earthquakes clearly triggered seismicity near the CTAO station (Table 2.1). Figure 2.11 shows a polar histogram of the distribution of the triggered events, where the observed incident angles for these triggering events (Figure 2.11) highly correlate with the angle predicted by our model (Figure 2.10). Four events arrived at $\alpha = 45 \pm 10^{o}$, three events arrived close to $\alpha = -45 \pm 12^{o}$, and one event $\alpha = 109^{o}$. Figure 2.12 shows the overlap of the angular distribution of the observed triggering events with the predicted potentials, relative to the average local stress for the reverse faults. These results demonstrate that stress from seismic surface

waves can be modeled using Coloumb Failure criteria to estimate their potential to trigger seismicity on fault planes of arbitrary orientation.

2.7 DISCUSSION

Our modeling allows for the calculation of the dynamic contributions to the shear and normal stresses on a fault plane of arbitrary orientation caused by the passing of the surface waves. Two aspects of the modeling become evident from our analysis: First, in concordance with the Coulomb failure criteria, we can argue that dynamic triggering of seismicity depends on both compressional/dilatational (normal stress) and shearing changes acting together in a suitable manner, dilatation unclamping the fault and facilitating the slip driven by shearing stresses, an interaction that is well represented by the triggering potentials. Second, in order to precisely quantify the contribution of normal and shear stress caused by the seismic waves to the fault local stress, the rotation of the dynamic stress tensor is essential. For example, Love waves are in general related to changes in the shear stress with no contribution to the normal stress. However, this only applies to the planes orthogonal to the vertical, transverse, and radial direction relative to the wave propagation. Love waves can cause changes on a fault plane's normal stress depending on orientation as showed in Figure 2.3, which extends the work of Hill et al. (2008) and gives us new insight into this failure process.

One difficulty in identifying the seismic phase responsible for triggering is that not all triggered events appear at exactly at the same time as the triggering phase in the seismogram. This may be due to the difference in path of the triggering and triggered waves to the station, permanent damage done to a fault contacts changing the frictional properties of the fault and accelerating failure (e.g., Parsons, 2005). If we know the type of faulting mechanism and the orientation of the triggered fault plane, the triggering potential can be used to estimate what wave

and what time section has the highest triggering potential for that specific fault, and therefore, was the most likely to have triggered the failure. Triggering delay is usually explained on a rate- and delay- frictional law basis (Parson, 2005). However, our modeling, along with a large number of real observations, could help to estimate to what extent changes in the Coulomb stress damage changes the frictional properties of the fault.

Even more challenging is to calculate determining the relatively small triggering dynamic stresses to the much larger driving local stresses. To address this, more precise local stress models and better and more complete dynamic stress models are required. In the case of the Bowen region, we had a number of observations and we were able to compare them to the modeled potential corresponding to a single wave of specific characteristics. In order to estimate a local-dynamic stress, it is necessary to calculate a potential threshold for triggering, which will require a more complete analysis considering the individual characteristics of the triggering and non-triggering waves. Similarly, to calculate the angle α for the observations, all triggered fault planes were considered to have a single orientation, the average faults' dip and strike suggested by (Hills et al., 1999). Alternatively, the horizontal mean stress orientation calculated by the Australian Stress Project (Hills et al., 1998) might be used to represent the direction perpendicular to normal faults strike; however, this does not give information on the dip of the faults. Ideally, individual triggered faults would be located and their real orientation used for the modeling. The introduction of this kind of parameter will be considered in future work.

2.8 CONCLUSION

Dynamic triggering may occur when surface waves passing through a previously overstressed fault plane change the fault local stress in a suitable manner. Modeling the potential that seismic waves have to trigger faulting at remote distance constitutes an important tool for

the understanding of the dynamic triggering phenomena. Our modeling allows for the calculation of the dynamic contributions to the shear and normal stresses on a fault plane of arbitrary orientation.. These potentials might be used, for example, to estimate what kind of faulting is more likely to be triggered by every part of a passing surface wave. Alternatively, the potentials could constrain the kind of wave (and direction of propagation) that is most likely to trigger faulting on a specific fault or fault region. As an example, we show that seismicity in the Australian Bowen region is more likely to be triggered by Love waves arriving at 45º from the average local compressive stress orientation. Observed events similar to those predicted by the modeled potentials demonstrate that our model suitably represents the stress caused by the passing of the surface waves and that dynamic triggering seismicity can be explained on Coulomb stress basis. The study of the local static–dynamic stress interaction will lead to a better understanding of the fault cycle, and at some point, dynamic triggering events could be used as a regional local stress indicator.

LIST OF REFERENCES

Anderson, J. G., J. N. Brune, J. N. Louie, Y. Zeng, M. Savage, G. Yu, Q. Chen, and D. dePolo (1994). Seismicity in the western Great Basin apparently triggered by the Landers, California earthquake, 28 June 1992, *Bull. Seism. Soc. Am., 84*, 863-891.

Arfken, G. B. and H. J. Weber (1996). Mathematical methods for physicists. Forth Edition, Academic Press 188-189, 1017.

Bosl, W., and A. Nur (2002). Aftershocks and pore diffusion following the 1992 Landers earthquake, *J. Geophys. Res*., 107 (B12), 2366, doi:10.1029/2001JB000155.

Brodsky, E. E., and S. G. Prejean (2005). New constraints on mechanisms of remotely triggered seismicity at Long Valley Caldera, *J. Geophys. Res*., 110, B04302, doi:10.1029/2004JB003211.

Brodsky, E. E., E. Roeloffs, D.Woodcock, I. Gall, and M. Manga (2003). A mechanism for sustained groundwater pressure changes induced by distant earthquakes, *J. Geophys. Res.*, 108(B8), 2390, doi:10.1029/ 2002JB002321.

Brodsky, E. E., V. Karakostas and H. Kanamori (2002). A new observation of dynamically triggered regional seismicity: Earthquakes in Greece following the August, 1999 Izmit, Turkey earthquake, *Geophys. Res. Lett., 27*, 2741-2744.

Brune, J. N., S. Brown, and P. A. Johnson (1993). Rupture mechanism and interface separation in foam rubber model earthquakes: A possible solution to the heat flow paradox and the paradox of large overthrusts, *Tectonophysics*, 218, 59-67.

Eberhart-Phillips, D, P. J. Haeussler, J. T. Feymueller, A. D. Frankel, C. M. Rubin, P. Craw, N. A. Ratchkovski, G. Anderson, G.A. Carver, A. J. Crone, T. E. Dawson, H. Fletcher, R. Hanson, E. L. Harp, R. A. Harris, D. P. hill, S. Hreinsdóttir, R. W. Jibson, L. M. Jones, R.

Kayen, D. K. Keefer, C. F. Larsen, S. C. Moran, S. F. Personius, G. Plafker, B. Sherroed, K. Sieh, N. Sitar, and W. K. Wallace (2003). The 2002 Denali fault earthquake, Alaska: A large magnitude, slip-partioned event, *Science*, 300, 1113-1118.

Gomberg, J., P. Bodin, K. Larson, and H. Dragert, (2004). Earthquake nucleation by transient deformations caused by the M = 7.9 Denali, Alaska, earthquake, *Nature, 427*, 621-624.

Gomberg, J., P. A. Reasenberg, P. Bodin, and R. A. Harris (2001). Earthquake triggering by seismic waves following the Landers and Hector Mine earthquakes, *Nature*, 411, 462–466.

Hill, D. P. (2008). Dynamic stresses, coulomb failure, and remote triggering, *Bull. Seismol. Soc. Am.*, 98, 66-92.

Hill, D. P., and S. G. Prejean (2007). Dynamic triggering, in Geophysical Treatise: Earthquake Seismology, edited by H. Kanamori, Elsevier, New York, in press.

Hill, D. P., P. A. Reasonberg, A. Michael, W. J. Arabasz, G. Beroza, J. N. Brune, D. Brumbaugh, R. Castro, S. Davis, D. dePolo, W. L. Ellsworth, J. Gomberg, S. Harmsen, L. House, S. M. Jackson, M. Johnston, L. Jones, R. Keller, S. Malone, L. Munguia, S. Nava, J. C. Pechmann, A. Sanford, R. W. Simpson, R. S. Smith, M. Stark, M. Stickney, A. Vidal, S. Walter, V. Wong, and J. Zollweg (1993). Seismicity in the western United States remotely triggered by the M 7.4 Landers, California, earthquake of June 28, 1992, *Science*, 260, 1617-1623.

Hillis, R. R., J. J. Meyer, and S. D. Reynolds (1998). The Australian stress map, *Exploration Geophysics*, 29, 420-427.

Hillis, R. R., J. J. Enever, and S. D. Reynolds. (1999). In situ stress field of eastern Australia, *Australian Journal of Earth Sciences*, 46, 813-825.

Husen, S., S. Wiemer, and R.B. Smith (2004). Remotely triggered seismicity in the Yellowstone National Park region by the 2002 Mw=7.9 Denali Fault Earthquake, Alaska, *Bull. Seismo. Soc. Am., 94*, S317-S331.

Leonard, G.S., Johnston, D.M., Paton, D., Christianson, A., Becker, J. & Keys, H. 2008 Developing effective warning systems: Ongoing research at Ruapehu volcano, New Zealand. *Journal of Volcanology and Geothermal Research,* 172: 199-215.

Linde, A. T., and I. S. Sacks (1998). Triggering of volcanic eruptions, Nature, 395, 888– 890.

Parsons, T., (2005), A hypothesis for delayed dynamic earthquake triggering, *Geophysical Research Letters*, Vol. 32, L04302, doi:10.1029/2004GL021811.

Pankow, K. L., W. J. Arabasz, J. C. Pechmann, and S. J. Nava (2004). Triggered seismicity in Utah from the November 3, 2002, Denali Fault earthquake, *Bull. Seismo. Soc. Am., 94*, S332-S347.

Perfettini, H., J. Schmittbuhl, and A. Cochard, (2003). Shear and normal load perturbations on a two-dimensional continuous fault: 2. Dynamic triggering. *J. Geophys. Res.*, 108(B9), 2409, doi:10.1029/2002JB001805.

Prejean, S. G. , D. P. Hill, E. E. Brodsky, S. E. Hough, M. J. S. Johnston, S. D. Malone, D. H. Oppenheimer, A. M. Pitt, and K. B. Richards-Dinger (2004). Remotely triggered seismicity on the United States west coast following the M 7.9 Denali Fault earthquake, *Bull. Seismo. Soc. Am*. 94, S348-S359.

Reid, H. (1910). Permanent displacements of the grounds: *in* The California Earthquake of April 18, 1906, Report of the State Earthquake Investigation Commission, v. 2, Carnegie Institution of Washington, Washington, D.C., p. 16-32.

Steacy, S., J. Gomberg, and M. Cocco (2005). Introduction to special section: Stress transfer, earthquake triggering, and time-dependent seismic hazard, *J. Geophys. Res.*, 110, B05S01, doi:10.1029/2005JB003692.

Stein, S. and M. Wysession (2003). An Introduction to Seismology, Earthquakes, and Earth Structure, *Malden, M.A., Blackwell Publishing Ltd.*, 86-92, 498.

Velasco, A. A., S. Hernandez, T. Parson and K. Pankow (2008). Global ubiquity of dynamic earthquake triggering, *Nature Geosciences*, 1, 375-379.

West, M., J.J. Sanchez, and S.R. McNutt (2005). Periodically triggered seismicity at Mount Wrangell, Alaska, after the Sumatra earthquake, *Science*, 308, 1144-1146.

TABLES

Table 2.1. Events that triggered seismicity at station CTAO near Australian Bowen Region.

Date	Event	Mw	Angle α (degrees)
03/25/1998	Balleny Island	8.1	109
11/16/2000	New Ireland	8.0	307
06/23/2001	Peru	8.4	54
07/13/2005	Tarapaca, Chile	7.8	53
09/25/2005	Northern Peru	7.5	48
05/03/2006	Tonga	8.0	24
01/13/2007	East Kuril	8.1	294
04/01/2007	Solomon	8.1	323

FIGURES

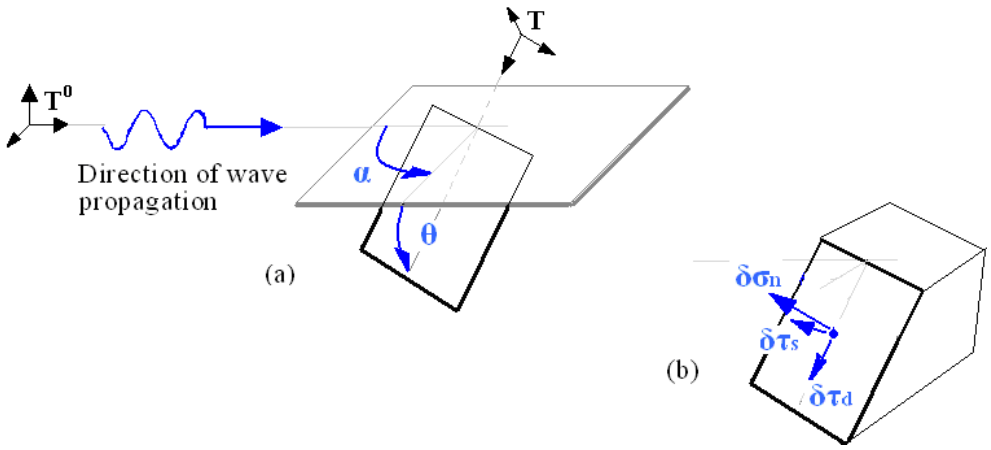

Figure 2.1 (a) The orientation of a fault plane relative to the direction of propagation of a seismic wave is defined in terms of angles alpha (α = 0-360°) and theta (θ = 0-90°). (b) $\delta\sigma_n$, $\delta\tau_s$, and $\delta\tau_d$ represent the stress changes caused by the passing of a seismic wave in the normal, strike, and dip direction respectively on the fault plane.

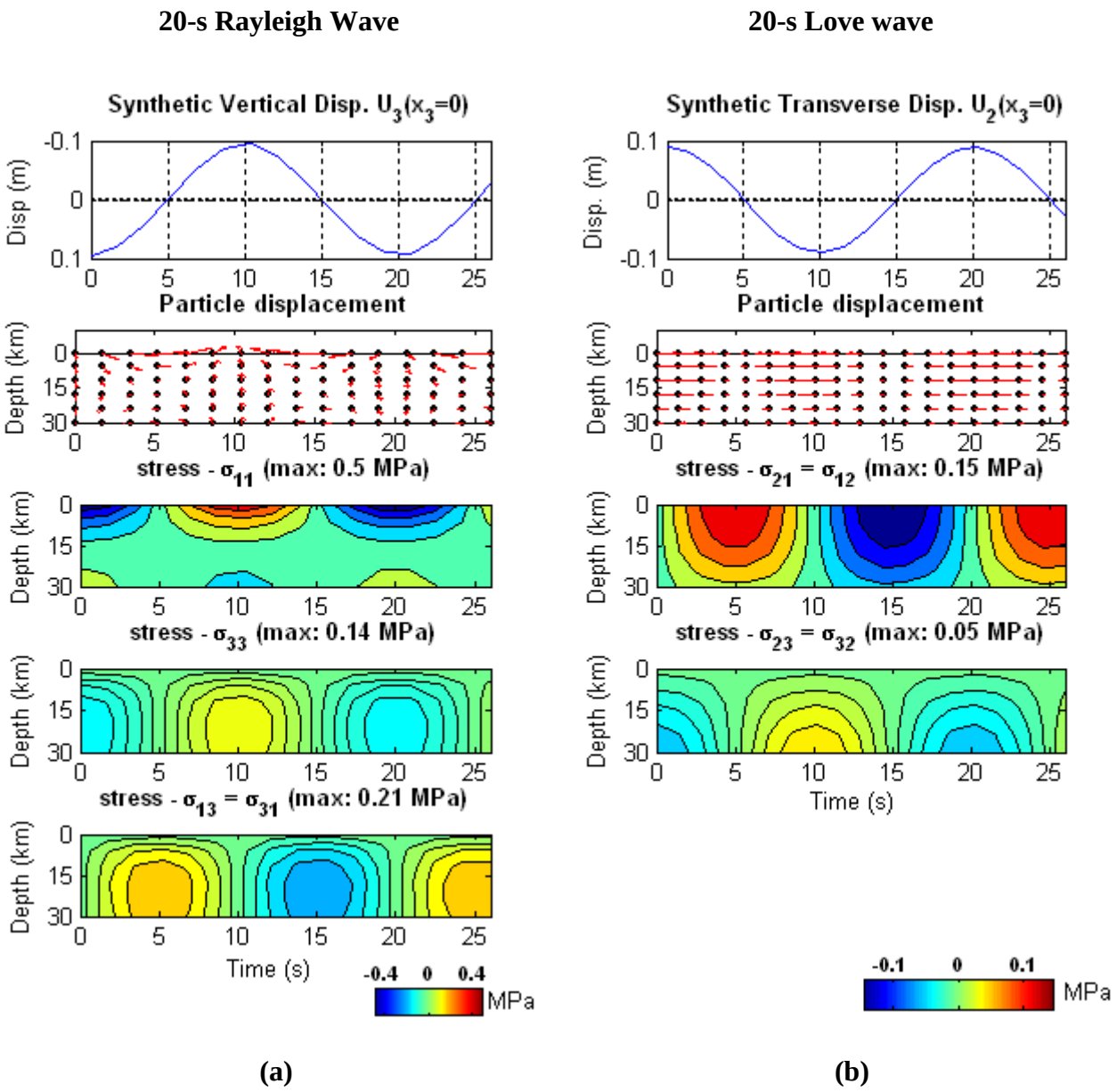

Figure 2.2. Synthetic Rayleigh and Love waves, and related stress components for a coordinate system with x_1 component in the direction of propagation, and x_3 in the depth direction. The color represents the magnitude and direction of the stress. For normal stress, the red color represents dilatation and blue represents compression. (a) (From top to bottom) Synthetic vertical displacement representing a 20-s period Rayleigh wave, related particle displacement, normal stress in the direction of wave propagation (σ_{11}), normal stress in

the vertical direction (σ_{33}), shear stress (σ_{13}). Note that σ_{11} decreases with depth, whereas σ_{33} and σ_{13} increase. (b) (From top to bottom) Synthetic transverse displacement representing a 20-s period Love wave, related particle displacement, and shear stresses (σ_{12}) and (σ_{23}). σ_{12} decreases with depth whereas σ_{23} increases.

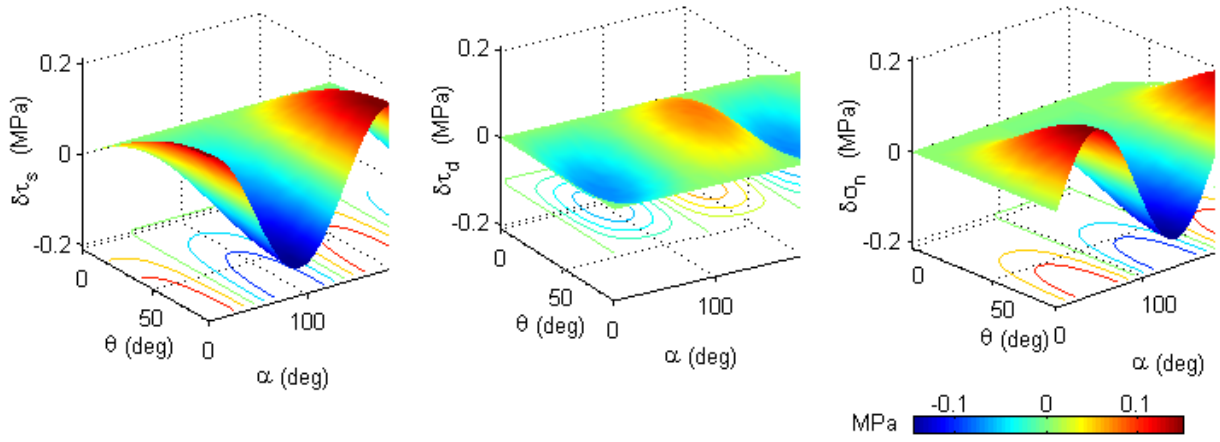

Figure 2.3. Example of the modeling of the dynamic stress that a Love wave, similar to that of Figure 2.2(a), will cause on a plane of arbitrary orientation *(α,θ)* as defined in Figure 2.1, for a depth D = 5 km and time = 5 s. $\delta\tau_s(\theta,\alpha)$, $\delta\tau_d(\theta,\alpha)$, and $\delta\sigma_n(\theta,\alpha)$ represent the contribution of the strike, dip and normal plane directions respectively. Notice that even though the Love wave induces only shear stresses on a coordinate system with one component in the direction of propagation and the other in the depth direction, the Love wave will cause a change in the normal stress ($\delta\sigma_n(\theta,\alpha)$) on rotated planes, reaching a maximum value for vertical planes (θ = 90º) striking 45º (α = 45º) from the direction of propagation.

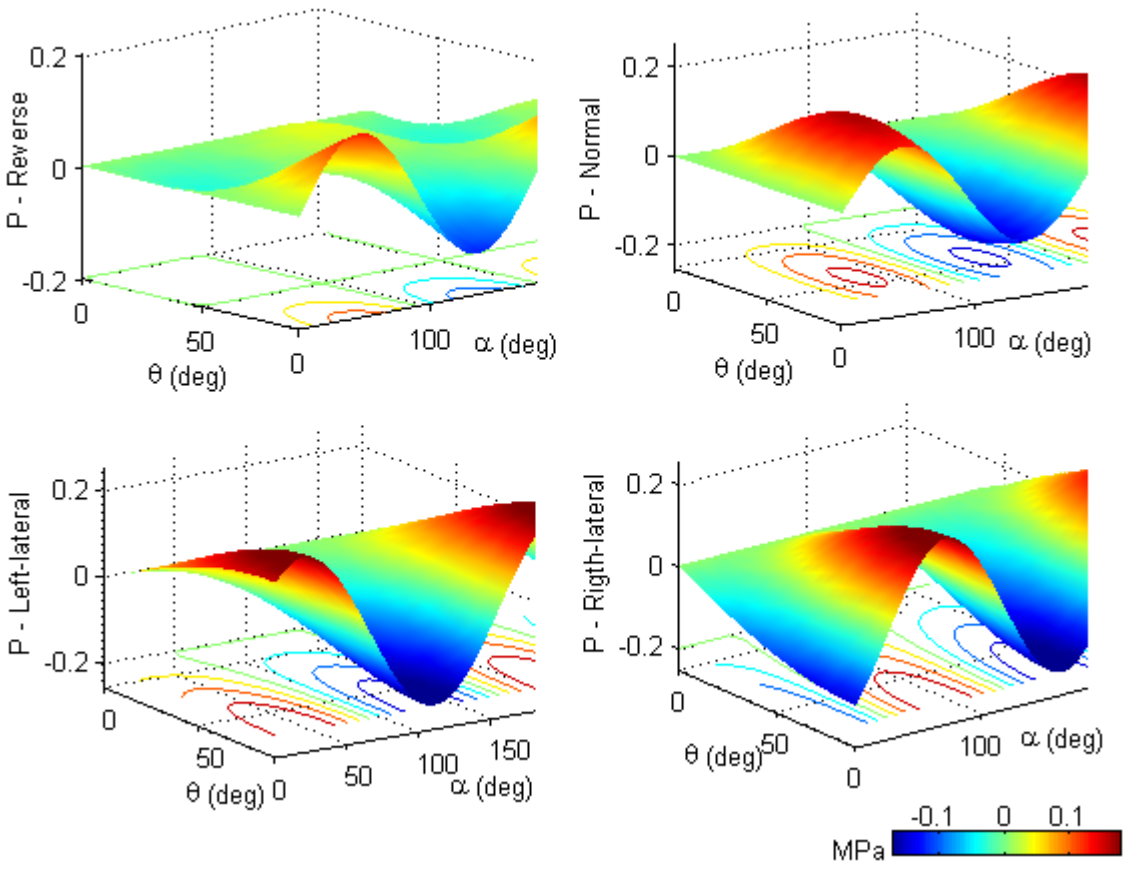

Figure 2.4. An example of triggering potentials modeling. Values in Figure 2.3 were used to calculate the potential of a 20-s period Love wave (similar to that in Figure 2.2(a)) to triggered reverse, normal, left- and right-lateral faulting. In this example we used a depth of 5 km, time equal to 5 s. (see figure 2.2(a)), and μ= 0.85. We plot only for α = 0-180 deg since there is a periodicity around α = 180 deg (in general α = 0-360 deg).

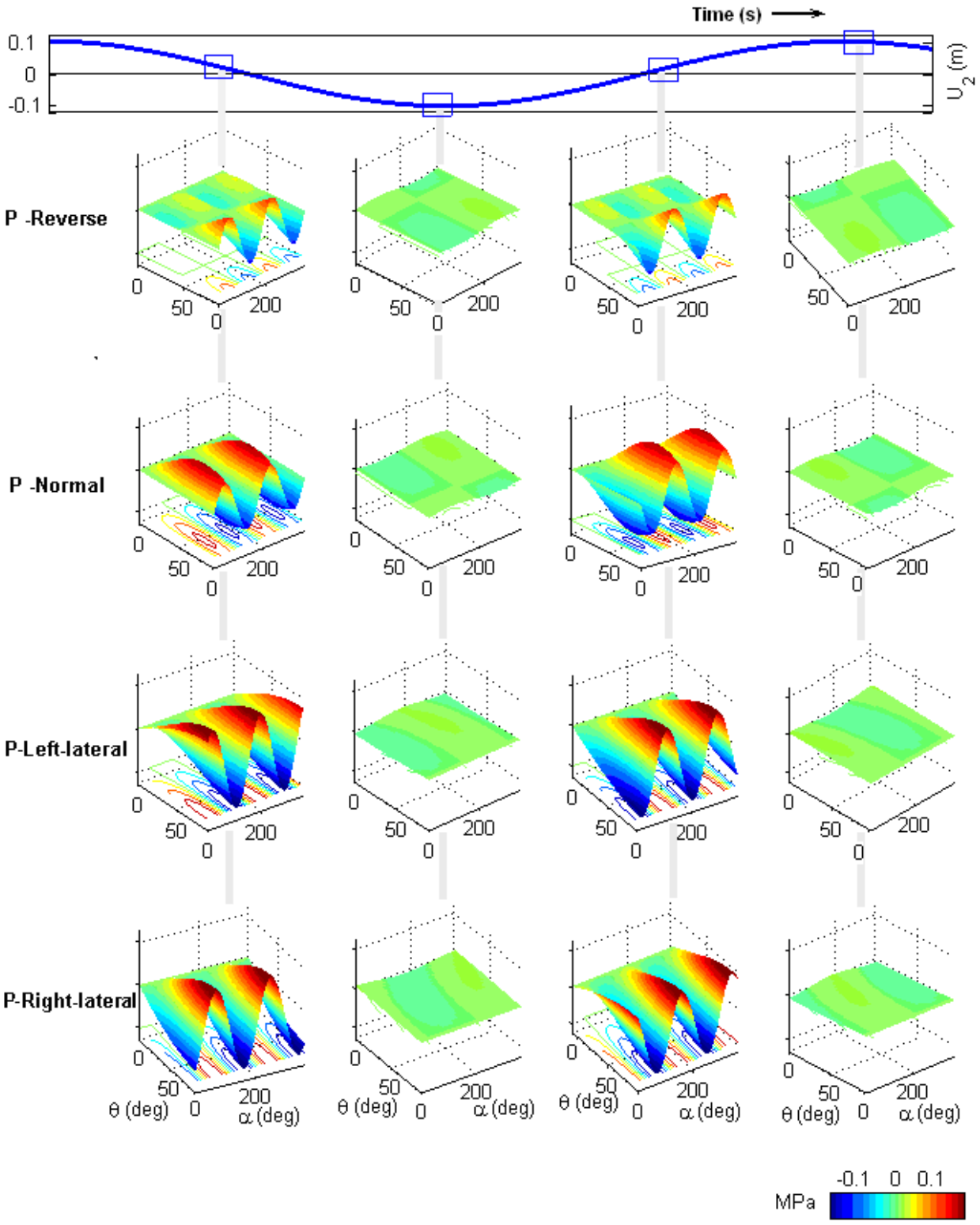
Time (s)
0.1
0
-0.1
U2 (m)
P -Reverse
P -Normal
P-Left-lateral
P-Right-lateral
0
50
200
θ (deg)
α (deg)
-0.1 0 0.1
MPa

Figure 2.5 (a)

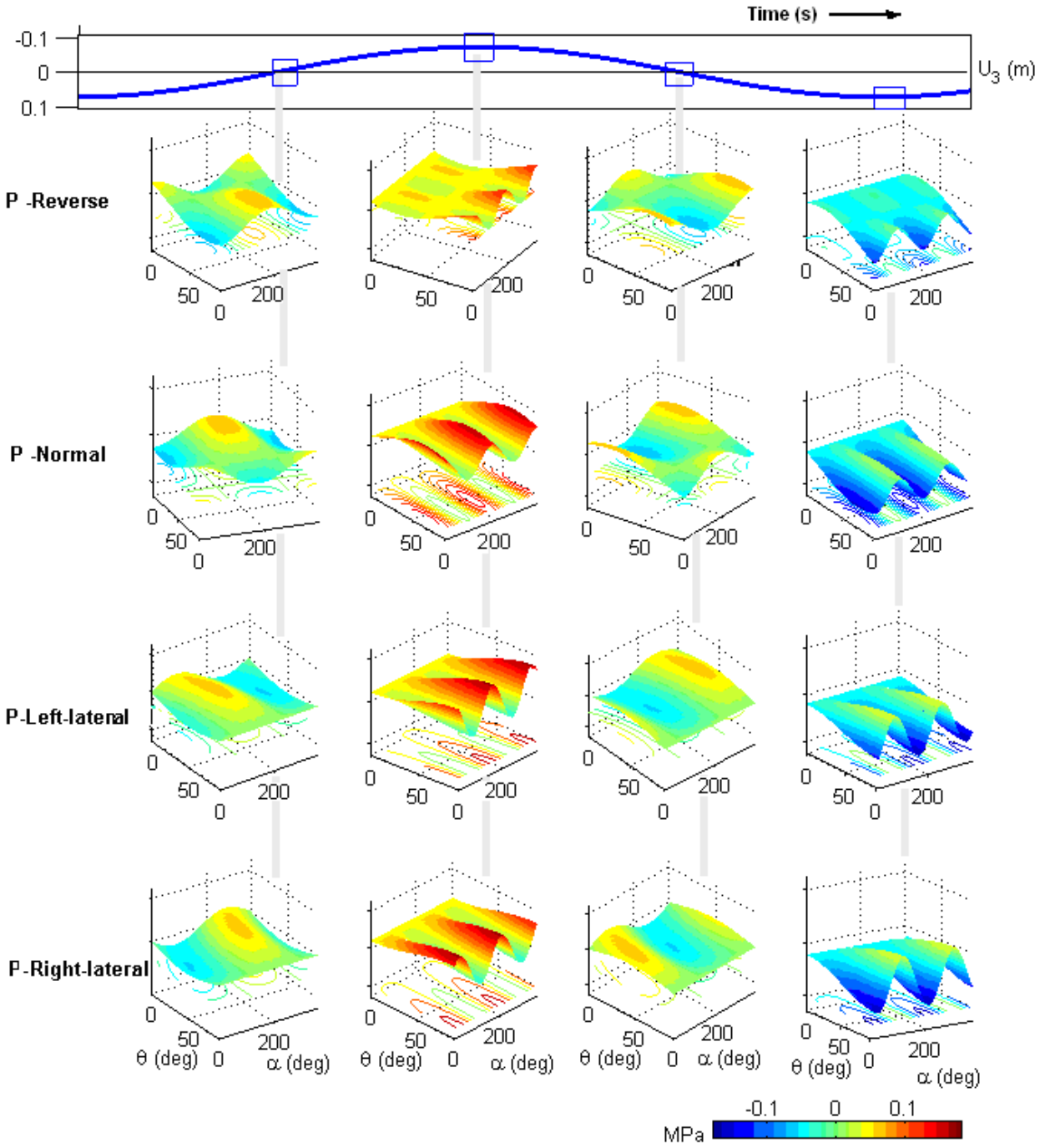
Time (s)
-0.1
0
0.1
U3 (m)
P -Reverse
P -Normal
P-Left-lateral
P-Right-lateral
0
50
200
θ (deg)
α (deg)
-0.1
0
0.1
MPa

Figure 2.5(b)

Figure 2.5. (a) Triggering potentials as function of fault plane orientation (α,θ) for a 20-s period Love wave at 5 km depth. The upper row shows the potentials of the wave to trigger reverse faulting for four key moments of the transverse motion: Negative-slope inflection, minimum, positive-slope inflexion, and maximum points (columns from left to right). Similarly, the second, third, and fourth rows are the potential to trigger normal, left-lateral, and right-lateral strike-slip faulting respectively. The same analysis is performed for four points of the vertical displacement of a 20-s period Rayleigh wave (b). By modeling the Love and Rayleigh waves related stress we can understand why a wave is more likely to trigger a specific kind of fault orientation over another, and why triggering occurs at a specific moment in time.

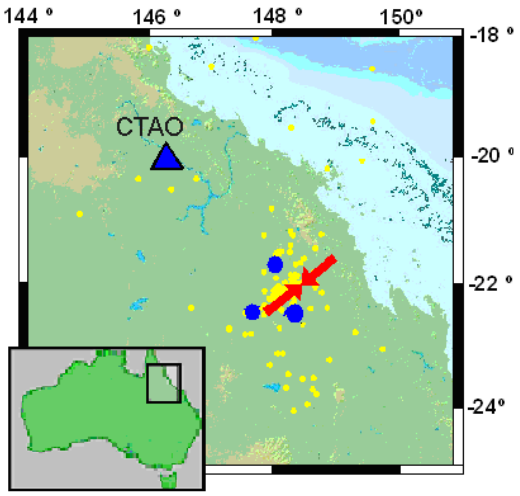

Figure 2.6. Australian Bowen region. Station CTAO.IU was used to identify dynamically triggered events, local seismicity since 1992 is shown by yellow dots, some of the possible triggered events are shown as blue circles, and average stress direction for the reverse faults mainly present in this region (maximum principal stress axis) is shown by red arrows.

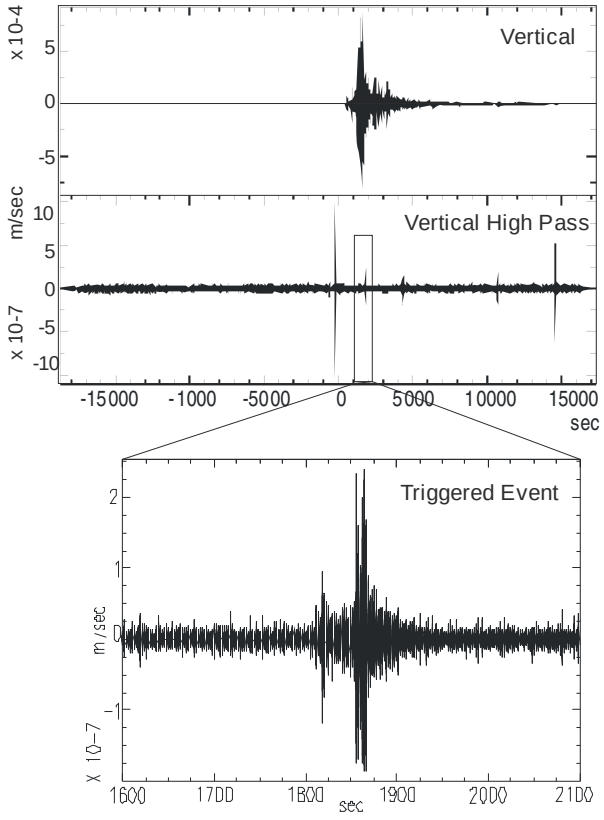

Figure 2.7. An example of identification of dynamic triggered events. (Top) Vertical displacement at the Australian CTAO.IU station caused by the seismic waves from the March 3rd 1998, Mw 8.1 Balleny Island event. (Middle) A 5 Hz high pass filter is applied to identify the high frequency local events triggered by the passing of the seismic waves. (Bottom) Magnification of a triggered event.

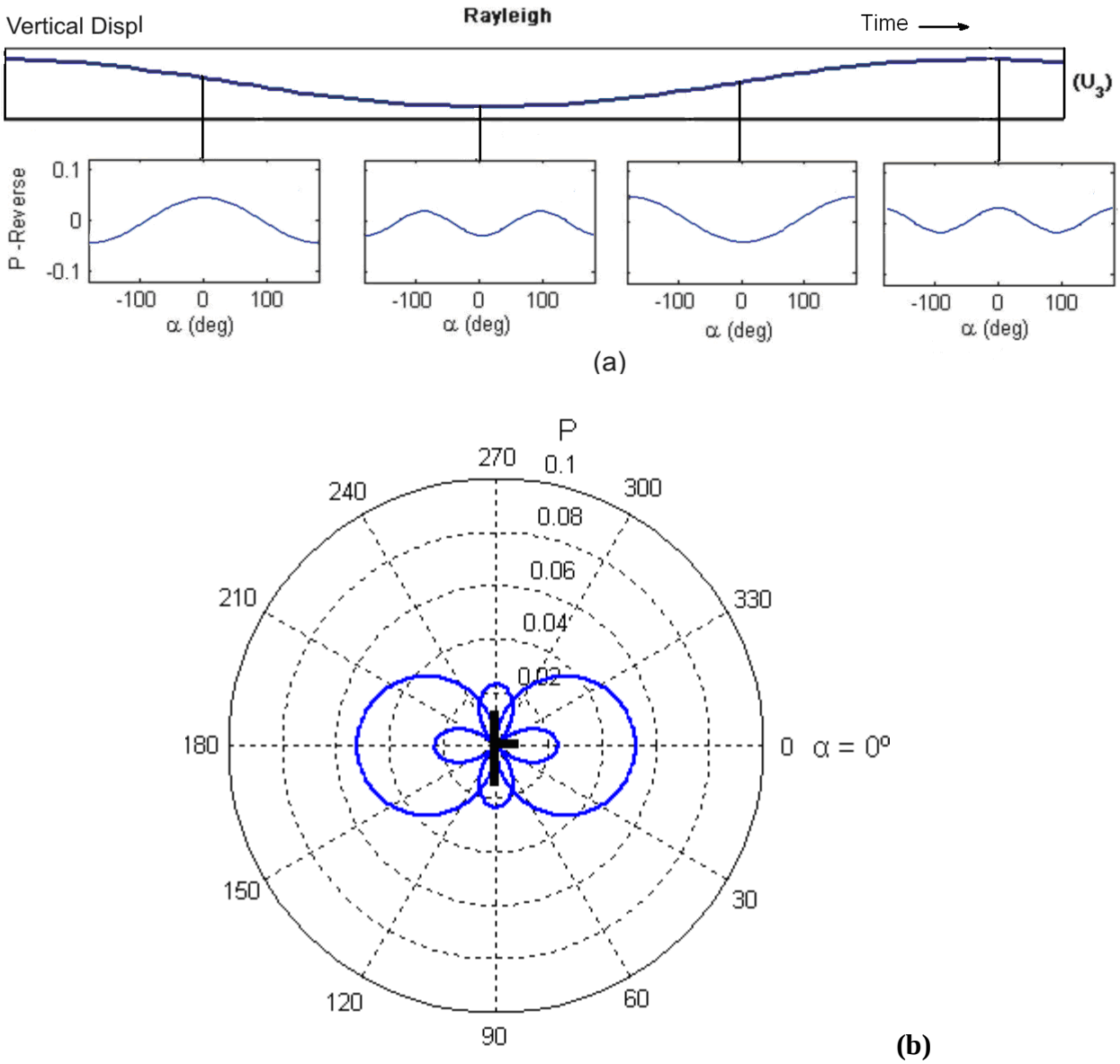

Figure 2.8. Triggering potential for Rayleigh wave corresponding to reverse faulting and θ = 70° as a function of time and α. (a) Maximum potential is reached at the negative inflection point in the vertical displacement (first panel from left to right), where the maximum occurs for waves arriving perpendicular to the strike of the fault planes (α = 0°). (b) Polar diagram shows the overall potential (for the whole wave time cycle) as function of α.

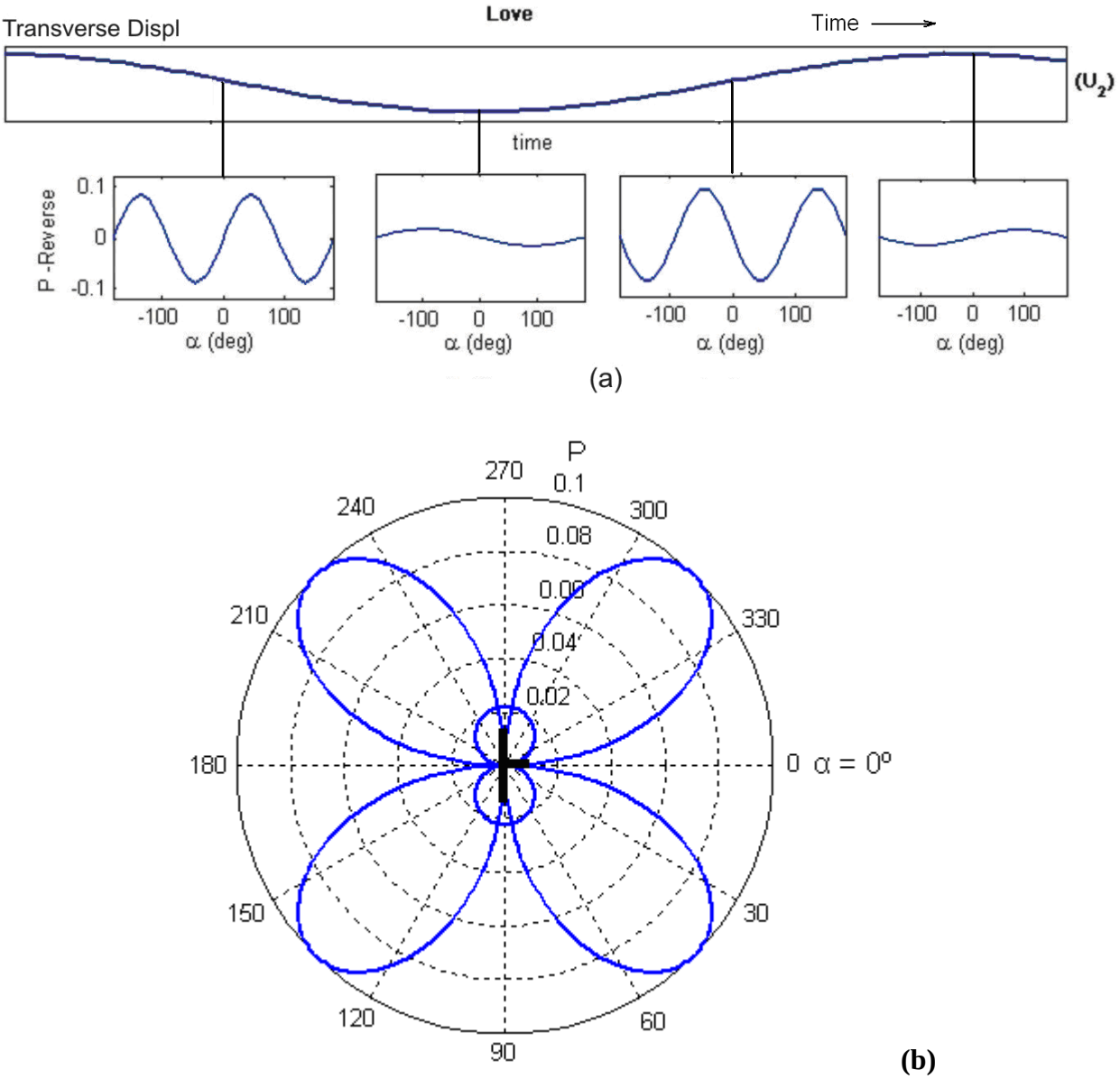

Figure 2.9. Triggering potential for Love wave corresponding to reverse faulting and θ = 70° as function of time and α. (a) Maximum potential of the Love waves occurs at the inflection points when waves arrive at 45° from the fault strike. (b) Polar diagram shows the overall potential (for the whole cycle) as function of α**.**

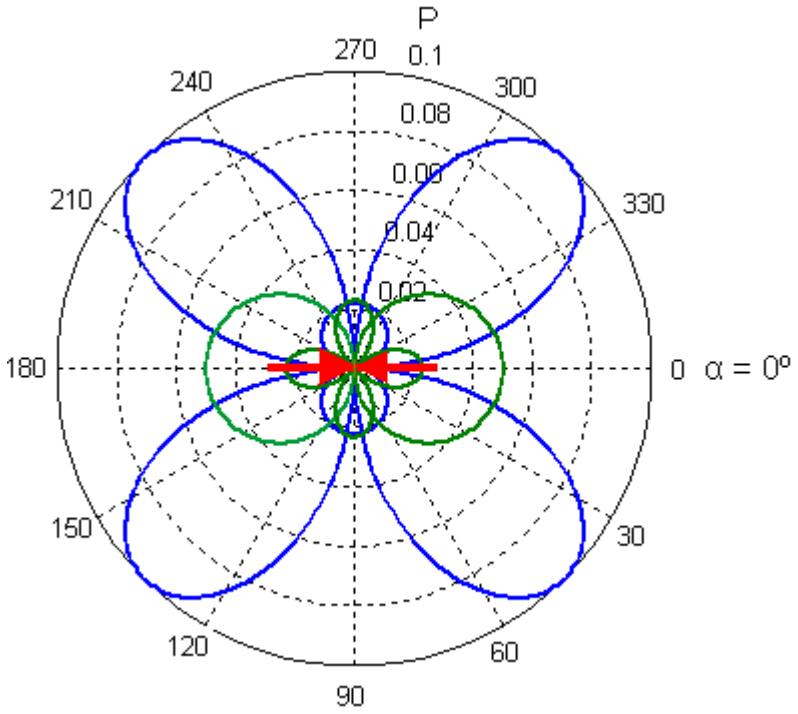

Figure 2.10. Figure shows the overlap of the Rayleigh wave's triggering potential (shown in green color) and the Love wave's potential (blue) relative to the average local compressive stress direction in the Bowen region (red arrows). Maximum potential is reached by Love waves arriving at 45° from the local stress, meaning that these waves are the most likely to trigger failure in the reverse faults present in this region.

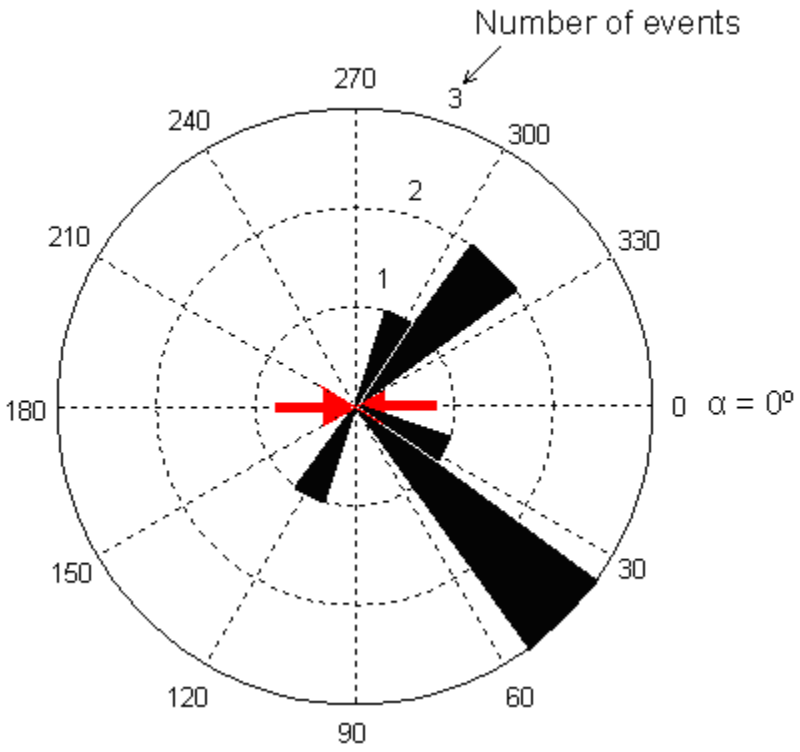

Figure 2.11. Histogram showing the distribution for the events found to have triggered seismicity in the Bowen region (histogram with group intervals of 20º).

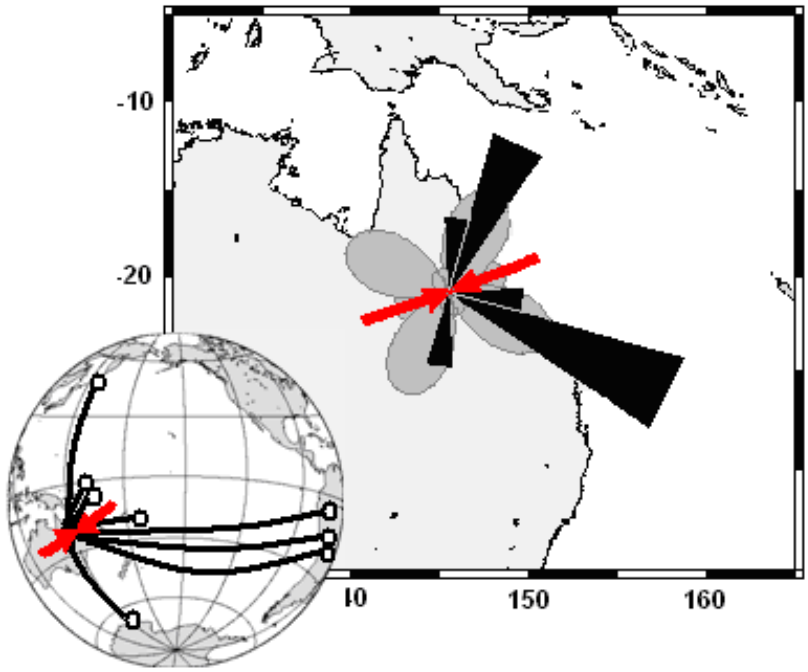

Figure 2.12. Inset shows the triggering events epicenters (open circle) and their ray paths to the Bowen region, along with the local compressional stress (red arrows) Figure shows the overlap of the angular distribution of the observed triggering events (black bins) with the predicted potentials (dark gray), and the average local stress for the reverse faults (red arrows).

CHAPTER 3

DYNAMIC STRESS MODELING FOR THE TRIGGERING OF NON-VOLCANIC TREMORS BENEATH THE CENTRAL RANGE IN TAIWAN

3.1 ABSTRACT

Seismic waves can trigger seismicity at great distance from the causable event. Recent studies have shown that the passing of seismic waves can trigger high frequency, low amplitude seismic signals with no clear body wave arrivals that occur away from volcanic regions, known as non-volcanic tremor (NVT). In this paper, we show how dynamic triggering of NVT can be modeled using a simple frictional approach based on a Coulomb failure criterion. Our modeling predicts the potential of a seismic wave to trigger slip on a fault plane promoting NVT. We search for tremor in the Central Range in Taiwan triggered by surfaces waves for ten large ($M_w \geq$ 7.5) earthquakes and compare the observations with our modeling. Four events triggered NVT: the 2002 Mw 7.8 2002 Kunlun earthquake, the 2003 Mw 8.3 Hokkaido earthquake, the 2004 Mw 9.0 Sumatra-Andaman earthquake, and the 2005 Mw 8.7 Sumatra-Indonesia earthquake. The orientation of the incoming waves appears to play a role in triggering, and both Rayleigh and Love waves promote triggering. In the case of the Kunlun event, modeling shows that Love waves promoted triggering, while for the Hokkaido and Sumatra events the Rayleigh waves promoted triggering of the NVT. A change in the Coulomb stress of ~2 kPa appears to be sufficient to trigger NVT in this region.

3.2 INTRODUCTION

Recent studies have shown that seismic waves can remotely trigger seismicity thousands of kilometers from an epicenter. This process is called dynamic. Dynamic triggering has been clearly documented for several large earthquakes including the 1992 Landers (M_w = 7.3) (Hill et al., 1993; Anderson et al., 1994;), the 2002 Denali Fault (M_w = 7.9) (Eberhart-Phillips et al., 2003; Gomberg et al., 2004; Husen and Wiemer, 2004; Pankow et al, 2004; Prejean et al., 2004), and the 2004 Sumatra (M_w = 9.15) (West et al., 2005; Velasco et al., 2008) earthquakes. Many studies on dynamic triggering seismicity focus on the triggering of small earthquakes on previously overstressed faults (e.g., Velasco et al., 2008). Recent studies have also demonstrate that non-volcanic tremor (NVT) can be triggered by seismic waves as well (Obara, 2002; Nadeau and Dolec, 2005; Miyazawa and Mori, 2006; Rubinstein et al., 2007; Gomberg et al., 2004; Miyazawa and Brosky 2008; Peng et al., 2008; Peng and Chao, 2008). NVT is usually observed in subduction zone and transform-fault environments away from volcanic regions, and it has a unique seismic signature. NVT is characterized by long duration, no clear body wave arrivals, and spectra depleted in high frequency energy compared with regular earthquakes with similar amplitude. NVT is commonly related to “slow-slip” events,. Slow-slip generally occurs so slowly that almost no seismic waves radiate. However, in some cases, slow-slip and tremor occur as a coupled phenomenon, and thus is termed ‘Episodic Tremor and Slip’ (ETS) (e.g., Shelly et al., 2006).

In this study, we develop a simple frictional approach based on a Coulomb failure criterion that has been shown to work for dynamically triggered earthquakes (Chapter 2) and apply this model to NVT. The model predicts the potential of a seismic wave to trigger slip on a fault plane, and we apply this modeling to four NVT triggered events that were identified in the

Central Range in Taiwan. The model appears to explain our observations. We found that the orientation of the incoming waves appears to play a role in triggering, and that both Rayleigh and Love waves promote triggering. A change in the Coulomb stress of ~2 kPa appears to be sufficient to trigger NVT in this region.

3.3 IDENTIFICATION OF TRIGGERED NVT

The collision of the Eurasian continental margin and the Luzon Arc results in the creation of the CR in Taiwan. Part of the deformation is consumed by lateral and thrust faulting along the Longitudinal Valley fault in eastern Taiwan. The rest is accommodated by the fold-thrust belt that forms the Western Foothills of the CR. Peng and Chao (2008) showed evidence of NVT beneath the Central Range (CR) in Taiwan triggered by the 2001 Mw 7.8 Kunlun earthquake. They hypothesized that NVT occurred on a weak basal detachment fault beneath the CR (Figure 3.1). The NVT location was calculated to be at 120.84º E ± 0.04 º and 23.10 º N ± 0.04 º underneath the CR in a transition zone between the locked and creeping portion of the basal detachment fault, and the depth is constrained at 19 ± 6 km. Peng and Chao (2008) suggests that the NVT triggered by the 2001 Kunlun event occurred on the subhorizontal decollement below the CR, so that the stress induced by the passing of the Love wave would result in southwest movement of the upper CR relative to the underlying Eurasian plate and the Luzon Arc (Figure 3.1), promoting lateral motion compatible with the local tectonic stress (Yu et al., 1997).

Inspired by Peng and Chao (2008) work, we performed a search for instances of dynamically trigged NVT in this region by other large earthquakes. We analyzed 10 events occurring between 2001 and 2005, within a radius of 90 º from the CR, and with Mw ≥ 7.5, (Table 3.1). We obtained three component seismograms from IRIS (Incorporated Research Institutions in Seismology) for the stations of the Broadband Array in Taiwan for Seismology

(BATS) shown in Figure 3.1. In order to identify NVT in the broadband spectrum of surfaces waves, a high-pass filter at 5 Hz was applied. Besides the 2001 Kunlun earthquake, previous study (Velasco, et. al., 2008) showed that three events have triggered NVT, the 2003 Hokkaido, the 2004 Sumatra, and the 2005 Sumatra earthquakes, shown in bold in Table 3.1 (Figure 3.2).

We hypothesize that NVT occurred beneath the CR in the same place or near the NVT triggered by the Kunlun earthquake. To address this, we calculate energy envelopes for all four events at all stations where NVT was observed (Figure 3.3). The envelope function is generated by taking envelopes of 5 Hz high pass filtered seismograms and smoothing using a moving average of 200 samples. A strong move-out of the envelopes of the NVT signal is observed for all stations that is similar between all events, suggesting that these signals are being generated at near that same source. Furthermore, the strongest signals are generated at the nearest stations (TBUP, TWGB) to the CR. We next model the stress caused by the passing of surface waves from the large events on the plane where the NVT was located and calculated their potential to trigger slip in the direction of the local stress, as described below.

3.4 FORMULATION OF THE MODELING

According to the Coulomb failure criterion, sliding on a fault plane will be promoted when stress increases in the direction of the fault local shear stress, and/or in the normal direction to the fault plane, unclamping the fault and facilitating shearing. For example, in Taiwan, local tectonic stress acts in the fault plane strike direction. Consequentially, if passing surface waves causes a change in this direction, say $+\delta\tau_s$, and/or in the normal direction unclamping the fault, say $+\delta\sigma_n$, sliding will be promoted. In such a case, the triggering potential, as defined by as the change in the Coulomb failure function will be positive:

$$P = \Delta CFF = \delta\tau_s + \mu\delta\sigma_n \quad (3.1)$$

where μ is known as coefficient of internal friction. A stress change in the direction opposite to the local shear stress ($-\delta\tau_s$) and/or in the normal direction ($-\delta\sigma_n$) clamping the fault, will move the fault away from sliding, and make the triggering potential (*P*) negative. Our goal is to calculate the magnitude and orientation of the change in the fault plane shear and normal stresses, caused by passing surface waves for triggered tremor events.

In general, the Rayleigh waves' related maximum stress components are normal stresses (compression/dilatation) in the radial direction (τ_{RR}) and in the vertical direction (τ_{ZZ}), and the shear stress (τ_{RZ}). Love waves generate only shear stresses (τ_{RZ} and τ_{TZ}). These stress components can be grouped into a dynamic stress tensor, which can be rotated to the fault plane to measure its contribution to the local shear and normal stress (Chapter 2), a contribution that depends on the fault plane orientation. This is done for both waves and for every peak and inflection point, then a quadratic interpolation is performed to represent the total potential as a function of time.

3.5 Stress Modeling and Observations

Figure 1 shows the location of stations and NVT. Since station TPUB appears to be the closest station to the NVT events, we model the ground displacement caused by the passing of the Love and the Rayleigh waves (as recorded by TPUB station transverse and vertical components, respectively) from the four large triggering earthquakes, and calculate the change that this displacement caused in the fault plane shear ($\delta\tau_s$) and normal stress ($\delta\sigma_n$). The triggering potential (*P*), as defined in by equation 3.1, was then calculated. We correlate each

observed NVT at a single station with calculated P, and estimate possible triggering mechanisms for every triggered event.

5.5.1 THE 2001 MW 7.8 KUNLUN EARTHQUAKE

The November 14, 2001, Mw 7.8 Kunlun earthquake occurred in northeastern Tibet along the western segment of the left-lateral Kunlun strike-slip fault system and produced a surface rupture of ~400 km, with the fault plane dipping 61° to the south and a location 200 km east of the rupture initiation (Ozacar and Beck, 2004). We model the transverse and vertical displacement caused by the Love and Rayleigh waves generated by the Kunlun earthquake near the CR and we calculate their contribution to the shear and normal stress, and triggering potential (Figure 3.4). We choose the triggered fault plane orientation from Peng and Chao (2008). We closely match the data with our synthetics (Figure 3.4), and show the changes in the shear and normal stress caused by the Love wave and Rayleigh wave, plus the sum (labeled as total) of the contributions by the two waves in the shear direction and the sum of the two contributions in the normal direction. Figure 3.4 also shows the P, where $\delta\tau_s$ is the total stress change in the shear direction (strike direction), $\delta\sigma_n$ is the total stress change in the normal direction, and μ is the coefficient of internal friction, we used $\mu = 0.1$ for this region (Suppe, 2007). We plot a dashed line to denote a possible threshold for the triggering potential of ~2 kPa, since in general, events that reached this potential caused; such that seismic waves causing a potential greater than 2 kPa are the most likely to trigger NVT on this fault plane.

For the Kunlun earthquake, the triggered NVT shows a good correlation with the calculated potential, which is dominated by the Love waves. In particular, the triggering potential reaches a maximum of ~25 kPa. Maximums in the triggering potential can be reached when the total shear stress ($\delta\tau_s$ *Total*) peaks (Figure 3.4). In this case, the potential is mostly created by the

shear stress since the contribution to normal stress ($\delta\sigma_n$ *Total*) is relatively weak. This total shear stress is caused almost entirely by the Love wave (as $\delta\tau_s$ *Rayleigh* is almost negligible). Also, the shear stress caused by Love wave peaks when the transverse displacement peaks. Love wave amplitude diminishes with depth and this vertical gradient in displacement results in horizontal shear in the displacement direction (τ_{TZ}), as shown in Figure 3.5. Seismic waves from the Kunlun earthquake arrive almost perpendicularly to the strike of the fault and the fault. Thus, the change in the shear stress in the strike direction $\delta\tau_s$ (and so the triggering potential) is almost totally caused by the τ_{TZ} component of the Love wave (as predicted by Peng and Chao, 2008).

3.5.2 THE 2003 MW 8.3 HOKKAIDO EARTHQUAKE

The September 25, 2003, Mw 8.3 Hokkaido earthquake was located about 60 km offshore and occurred as the result of thrust-faulting on the plate interface between the overriding North American plate and the subducting Pacific plate. NVT in Taiwan triggered by the Hokkaido event also correlate with peaks in the triggering potential. In this case, a maximum potential of ~10 kPa is reached (Figure 3.6) and there is a more equitable contribution to the total normal ($\delta\sigma_n$ *Total*) and total shear stress ($\delta\tau_s$ *Total*). Figure 3.6 also shows that total normal stress correlates with the Rayleigh wave vertical displacement, since this part of the wave causes large changes in the vertical and radial normal stress. However, the potential is in phase with the shear stress because of the low contribution of the normal stress to the potential as a result of the low value of coefficient of friction μ (0.1). The total shear stress is almost completely caused by the Rayleigh wave (as $\delta\tau_s$ is relatively low). Figure 3.6 also shows that Rayleigh wave shear stress (and potential) correlates with the positive inflection points for the vertical displacement. The negative inflection points for the Rayleigh wave correspond to positive inflection points in

space. This part of the Rayleigh has a shear stress component acting on a horizontal plane in the direction of propagation (Figure 3.7). The seismic waves from this event arrive almost parallel to the strike of the fault plane (τ_{RZ}). This stress component is thus likely responsible for the change in the shearing in the strike direction and for the triggering.

3.5.3 THE 2004 MW 9.0 SUMATRA-ANDAMAN AND THE 2005 MW 8.7 SUMATRA-INDONESIA EARTHQUAKES

The December 26, 2004 (Mw 9.0) Sumatra-Adams earthquake occurred as thrust-faulting on the interface of the India plate and the Burma plate. The width of the earthquake rupture, measured perpendicular to the Sunda trench, is estimated to have been about 150 km and the maximum displacement on the fault plane was about 20 meters. This is the fourth largest earthquake that has occurred since 1900 and is the largest since the 1964 Prince William Sound, Alaska earthquake. The March 28, 2005 (Mw 8.6) Sumatra-Indonesia earthquake generated a rupture length of about 500 kilometers. The epicenter was located approximately 200 km southeast of the December 2004 epicenter.

In the case of both the 2004 earthquake (Figure 3.8) and the 2005 earthquake (Figure 3.9), the modeled triggering potentials correlate well with the NVT recordings. For the 2004 earthquake, the maximum potential is ~15 kPa, while for the 2005 event the maximum potential was ~8 kPa. In both cases, a relatively equal contribution to the shear ($\delta\tau_s$ *Total*), and normal ($\delta\sigma_n$ *Total*) stress was observed. As seen for the other events, the relatively low coefficient of friction μ (0.1) causes the shear stress to be responsible for the triggering. Given the large rupture length of the 2004 earthquake, the azimuth of the arrival phases is likely to vary by several degrees. Nonetheless, the higher potential for the 2004 event results from the higher ground displacement rather than azimuthal direction since both epicenters lie relatively close to

each other. For both of these events, the Rayleigh waves appear to be responsible for the triggering stresses; the shear stress (and potential) correlates with a positive inflection point in the vertical displacement. These inflection points correspond to a negative inflection point in space (Figure 3.10), which has a component of shear stress acting on a horizontal plane in the negative direction of propagation ($-\tau_{RZ}$) and contributes efficiently to the fault shear stress $\delta\tau_s$.

3.6 DISCUSSION

For four of the ten large earthquakes that we investigated, we discovered triggered NVT that we can model using simple Coulomb Failure criteria. From these events, we have shown that the direction of the incoming wave and the wave type play an important role in the ability to trigger earthquakes. Both Love and Rayleigh waves show potential for triggering earthquakes, and can contribute to additional shear stress that may cause a fault close to failure to trigger. Furthermore, the magnitude of the triggering stress appears to be important. To investigate this more closely, we discuss the events that did not trigger.

Figure 11 shows the seismic waves and related potentials for the six large events for which we did not find evidence of have triggered tremors beneath the CR in Taiwan. With the exception of the Mw 7.6 2005 Pakistan earthquake, which reached a maximum triggering potential of ~5 kPa (Figure 3.11), the triggering potential did not exceed 2 kPa. The Pakistan event should show a similar mechanism as the Kunlun earthquake, since high potential was manly due to Love waves arriving almost at the same direction as Love waves from Kunlun earthquake. However, the triggering potential for the Kunlun earthquakes was five times higher than for the Pakistan earthquake. Figure 3.12 shows the overlap of the potentials for the ten events. Dark color denotes the non-triggering events, while light colors are used for triggering events. In general, the threshold value for the triggering of tremors of 2 kPa matches our

observations relatively well. We propose a threshold in the change in the Coulomb stress of 2 kPa which of the same order with threshold for the triggering of NVT in the Long Valley Caldera (Brodsky and Prejean, 2005), and recent surveys of triggered tremor in Vancouver Island (Rubinstein et. al., 2009) and Taiwan (Peng and Chao, 2008).

If we are able to model the triggering using simple Coulomb Failure criteria, this implies that NVT is caused by movement along faults that are similar to typical earthquakes and are close to failure. Slow rupture could be the only difference from high frequency failure; NVT are shown to occur at depth where temperature and pressures are greater. For Taiwan, the original location by Peng and Chao (2008) was 19 km, which they suggest it occurred below the seismogenic zone. High confining pressures could play a role slowing slipping while high temperatures could cause a low coefficient of friction which would allow a gradual realizes of energy, opposite to earthquakes, where a rapid slip and high coefficient of friction cause a faster release of energy.

3.7 CONCLUSIONS

Dynamic triggering of seismicity may occur when the surface waves pass through a fault plane and change the fault's local stresses in a suitable manner. We show that dynamic triggering of NVT can be modeled based on a simple Coulomb frictional approach. We identified three large events besides the 2001 Kunlun earthquakes that have had triggered NVT beneath the CR in Taiwan: The 2003 Hokkaido, the 2004 Sumatra, and the 2005 Sumatra earthquakes. We modeled the stress caused by the surface waves from ten large earthquakes to investigate the stress conditions required to trigger NVT in this region. For the Kunlun earthquake, our modeling shows that the orientation and magnitude of the incoming Love wave contributes to increasing the fault plane local shear stress. In the cases of the Hokkaido and Sumatra

earthquakes, the orientation and magnitude of the incoming Rayleigh waves contribute to the shear local stress. In general, NVT correlates with peaks in our modeled triggering potential, and we suggest that a minimum threshold of ~2 kPa must be reached to trigger NVT.

LIST OF REFERENCES

Anderson, J. G., J. N. Brune, J. N. Louie, Y. Zeng, M. Savage, G. Yu, Q. Chen, and D. dePolo (1994). Seismicity in the western Great Basin apparently triggered by the Landers, California earthquake, 28 June 1992, *Bull. Seism. Soc. Am., 84*, 863-891.

Cheng C. -H.,Wang,W.-H.&Teng, T.-L. (2001). 3D velocity structure around the source area of the 1999 Chi-Chi, Taiwan, earthquake: before and after the mainshock, *Bull. seism. Soc. Am.*, **91,** 1013–1027.

Eberhart-Phillips, D, P. J. Haeussler, J. T. Feymueller, A. D. Frankel, C. M. Rubin, P. Craw, N. A. Ratchkovski, G. Anderson, G.A. Carver, A. J. Crone, T. E. Dawson, H. Fletcher, R. Hanson, E. L. Harp, R. A. Harris, D. P. hill, S. Hreinsdóttir, R. W. Jibson, L. M. Jones, R. Kayen, D. K. Keefer, C. F. Larsen, S. C. Moran, S. F. Personius, G. Plafker, B. Sherroed, K. Sieh, N. Sitar, and W. K. Wallace (2003). The 2002 Denali fault earthquake, Alaska: A large magnitude, slip-partioned event, *Science, 300*, 1113-1118.

Gomberg, J., P. Bodin, K. Larson, and H. Dragert (2004). Earthquake nucleation by transient deformations caused by the *M* w 7.9 Denali, Alaska, earthquake, *Nature,* 427, 621–624.

Gomberg, J. S., P. A. Reasenberg, P. Bodin, and R. A. Harris (2004). Earthquake triggering by seismic waves following the Landers and Hector Mine earthquakes, *Nature,* 411, 462–466.

Hill, D. P., P. A. Reasonberg, A. Michael, W. J. Arabasz, G. Beroza, J. N. Brune, D. Brumbaugh, R. Castro, S. Davis, D. dePolo, W. L. Ellsworth, J. Gomberg, S. Harmsen, L. House, S. M. Jackson, M. Johnston, L. Jones, R. Keller, S. Malone, L. Munguia, S. Nava, J. C. Pechmann, A. Sanford, R. W. Simpson, R. S. Smith, M. Stark, M. Stickney, A. Vidal, S. Walter, V. Wong, and J. Zollweg (1993). Seismicity in the western United States

remotely triggered by the M 7.4 Landers, California, earthquake of June 28, 1992, *Science,* 260, 1617-1623.

Husen, S., and S. Wiemer (2004). Remotely triggered seismicity in the Yellowstone National Park region by the 2002 *M*w7.9 Denali fault earthquake, Alaska, *Bull. Seism. Soc. Am.,* 94, no. 6B, S317–S331.

Miyazawa, M. and E.E. Brodsky (2008). Deep low-frequency tremor that correlates with the passing surface waves, *J. Geophys. Res.* 113, doi:10.1029/2006JB004890.

Miyazawa, M. and J. Mori (2006). Evidence suggesting fluid flow beneath Japan due to periodic seismic triggering from the 2004 Sumatra-Andaman earthquake, *Geophys. Res. Lett.* 33, L05303, doi:10.1029/2005GL025087.

Nadeau, R.M. and D. Dolenc (2005). Nonvolcanic tremors deep beneath the San Andreas Fault, *Science,* 307, 389.

Obara, K. (2002). Nonvolcanic deep tremor associated with subduction in southwest Japan, *Science,* 296, 1679–1681.

Ozacar, A. A., and S. L. Beck (2004). The 2002 Denali fault and 2001 Kunlun fault earthquakes: Complex rupture process of two large strike-slip events, *Bull. Seism. Soc. Am*. 94 ,S278 – S292.Pankow, K. L., W. J. Arabasz, J. C. Pechmann, and S. J. Nava (2004). Triggered seismicity in Utah from the November 3, 2002, Denali Fault earthquake, *Bull. Seismo. Soc. Am.*, 94, S332-S347.

Peng, Z. and K. Chao (2008) Non-volcanic tremor beneath the Central Range in Taiwan triggered by the 2001 *M*w 7.8 Kunlun earthquake, *Geophys. J. Int.*, 175, 825–829.

Peng, Z., J.E. Vidale, K.C., Creager, J.L. Rubinstein, J. Gomberg, & P. Bodin (2008).

Strong tremor near Parkfield, CA excited by the 2002 Denali earthquake, *Geophys. Res. Lett. Geophys. Res. Lett.* 35, L23305, doi:10.1029/2008GL036080.

Prejean, S. G. , D. P. Hill, E. E. Brodsky, S. E. Hough, M. J. S. Johnston, S. D. Malone, D. H. Oppenheimer, A. M. Pitt, and K. B. Richards-Dinger (2004). Remotely triggered seismicity on the United States west coast following the M 7.9 Denali Fault earthquake, *Bull. Seismo. Soc. Am,*. 94, S348-S359.

Rogers, G. and H. Dragert (2003). Episodic tremor and slip on the Cascadia subduction zone: the chatter of silent slip, *Science,* 300, 1942–1943.

Rubinstein, J.L., J. E. Vidale, J. Gomberg,, P. Bodin., K. C. Creager, and S. Malone (2007). Non-Volcanic Tremor Driven by Large Transient Shear Stresses, *Nature,* 448, 779-589.

Shelly, D. R., G. C. Beroza, S. Ide, and S. Nakamula (2006). Low-frequency earthquakes in Shikoku, Japan, and their relationship to episodic tremor and slip, *Nature,* 442, 188-191.

Stein, S. and M. Wysession (2003). An Introduction to Seismology, Earthquakes, and Earth Structure, *Malden, M.A., Blackwell Publishing Ltd.*

Suppe, J. (2007). Absolute fault and crustal strength from wedge tapers, *Geology* 35(12), 1127–1130; doi:10.1130/G24053A.1.

Velasco, A. A., S. Hernandez, T. Parson and K. Pankow (2008). Global ubiquity of dynamic earthquake triggering, *Nature Geosciences,* 1, 375-379.

West, M., J.J. Sanchez, and S.R. McNutt (2005) Periodically triggered seismicity at Mount Wrangell, Alaska, after the Sumatra earthquake, *Science,* 308, 1144-1146.

Yu, S.B., H. Y. Chen, and L. C. Kuo (1997). Velocity field of GPS stations in the Taiwan area, *Tectonophysics,* 274, 41–59.

TABLES

Table 3.1 List of events used in this study. Triggering events are denoted by bold type.

Event	Date (year mo day)	Time (hr min sec)	Latitude	Longitude	Mw
Kunlun, China	**2001 11 14**	**09:26:10**	**35.946**	**90.541**	**7.8**
Mindanao	2002 03 05	21:16:09	6.03	124.24	7.5
New Guinea	2002 09 08	18:44:26	-3.228	142.87	7.6
Irian, Jaya, Indonesia	2002 10 10	10:50:20	-1.707	134.165	7.6
Denali Fault, AK	2002 11 03	22:12:41	63.52	-147.53	7.9
Hokkaido, Japan	**2003 09 25**	**19:50:06**	**41.81**	**143.91**	**8.3**
Macquarie Ridge	2004 12 23	14:59:03	-50.14	169.36	8.1
Sumatra-Andaman	**2004 12 26**	**00:58:53**	**3.3**	**95.96**	**9.0**
Sumatra-Indonesia	**2005 03 28**	**16:09:36**	**2.074**	**97.013**	**8.7**
Pakistan	2005 10 08	03:50:40	34.493	73.629	7.6

FIGURES

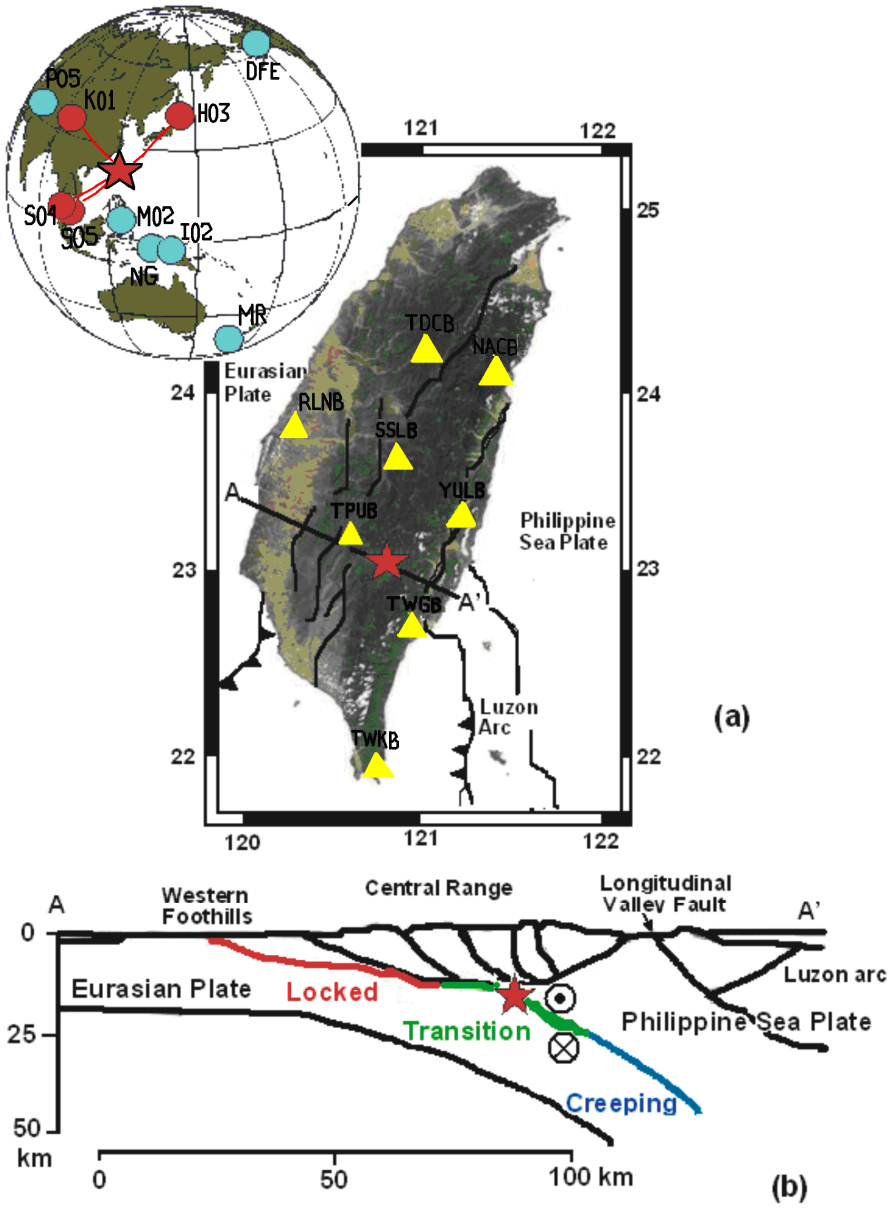

Figure 3.1. Central Range (CR) region in Taiwan. (a) The inset shows the epicenters of the large earthquakes used to investigate the triggering of NVT beneath the CR in Taiwan. Red circles represent triggering events and blue circles non-triggering events. Red star represents the location of tremor. Map shows location the BATS

stations used to identify tremor hidden in the large events' surface waves. (b) A schematic cross-section of geological features in southern Taiwan along AA' (as defined in (a)). The red and blue color mark the locked and creeping portion of the basal detachment fault, respectively, whereas the green color denotes the transition zone where triggered tremor occurs. The direction of triggered lateral slip is defined by circle symbols; Modified from Peng and Chao, (2008). Key for earthquakes in inset: K01 – 2001, Mw 7.8 Kunlun, China; M02 – 2002, Mw 7.5 Mindanao; NG – 2002, Mw 7.6 New Guinea; I02 – 2002, Mw 7.6 Irian, Java, Indonesia; DFE – 2002, Mw 7.9 Denali Fault; H03 – 2003**,** Mw 8.3 Hokkaido, Japan; MR – 2004, Mw 8.1 Macquarie Ridge; S04 – 2004, Mw 9.0 Sumatra-Andaman; S05 – 2005, Mw 8.7 Sumatra-Indonesia; P05 – 2005, Mw 7.6 Pakistan.

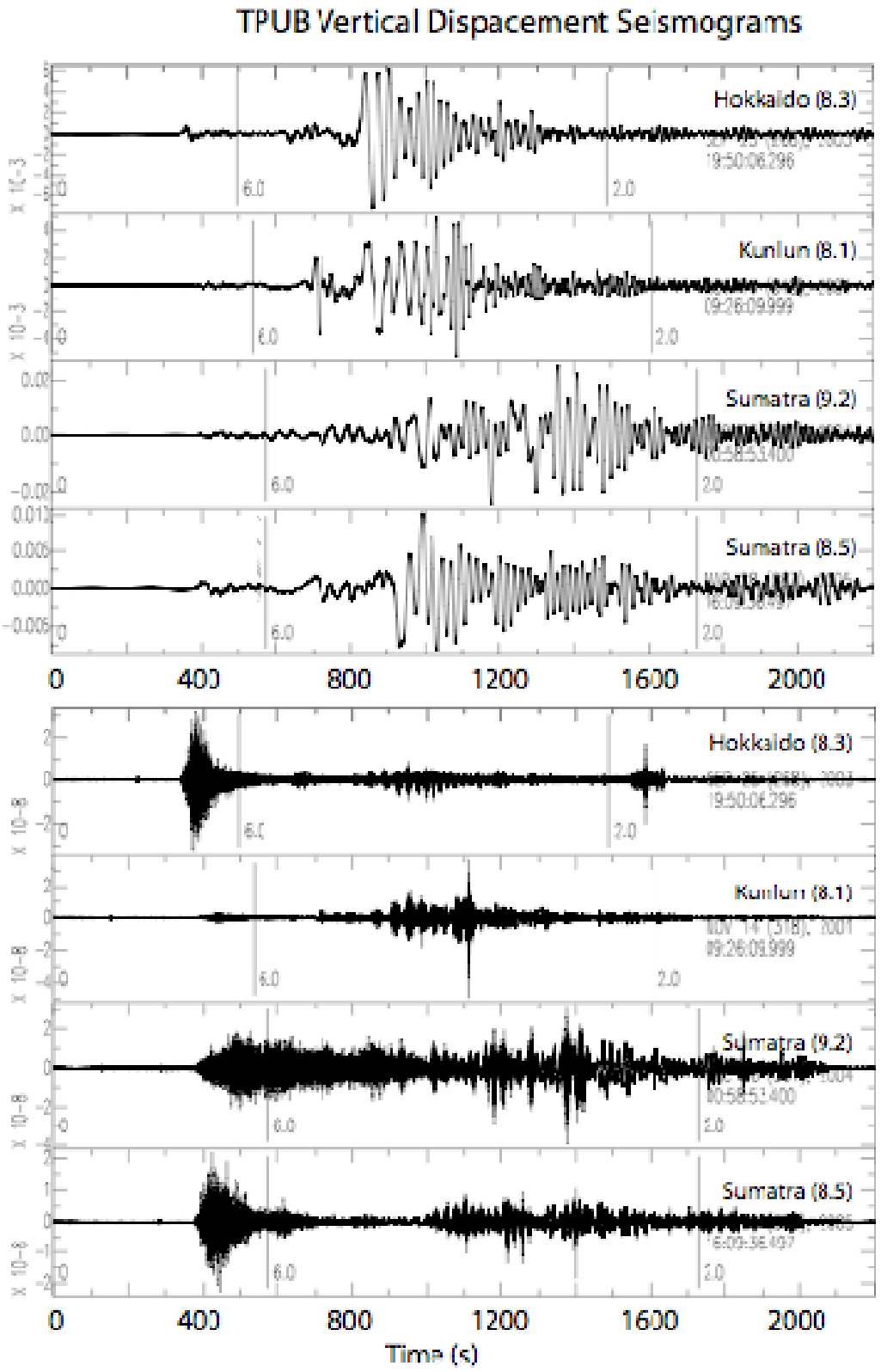
TPUB Vertical Dispacement Seismograms
Hokkaido (8.3)
Kunlun (8.1)
Sumatra (9.2)
Sumatra (8.5)
0
400
800
1200
1600
2000
Hokkaido (8.3)
Kunlun (8.1)
Sumatra (9.2)
Sumatra (8.5)
0
400
800
1200
1600
2000
Time (s)

Figure 3.2. Vertical-component, broadband displacement waveforms recorded at seismic station TPUB in Taiwan for four large earthquakes that triggered NVT (2003 Mw 8.1 Hokkaido, 2001 Mw 8.1 Kunlun, 2004 Mw 9.2 Sumatra, and 2005 Mw 8.5 Sumatra). The top traces are unfiltered displacement seismograms, and the bottom traces are high pass filtered. Note the triggered NVT in the high pass filtered (at 5 Hz) traces that correspond to the passing surface waves.

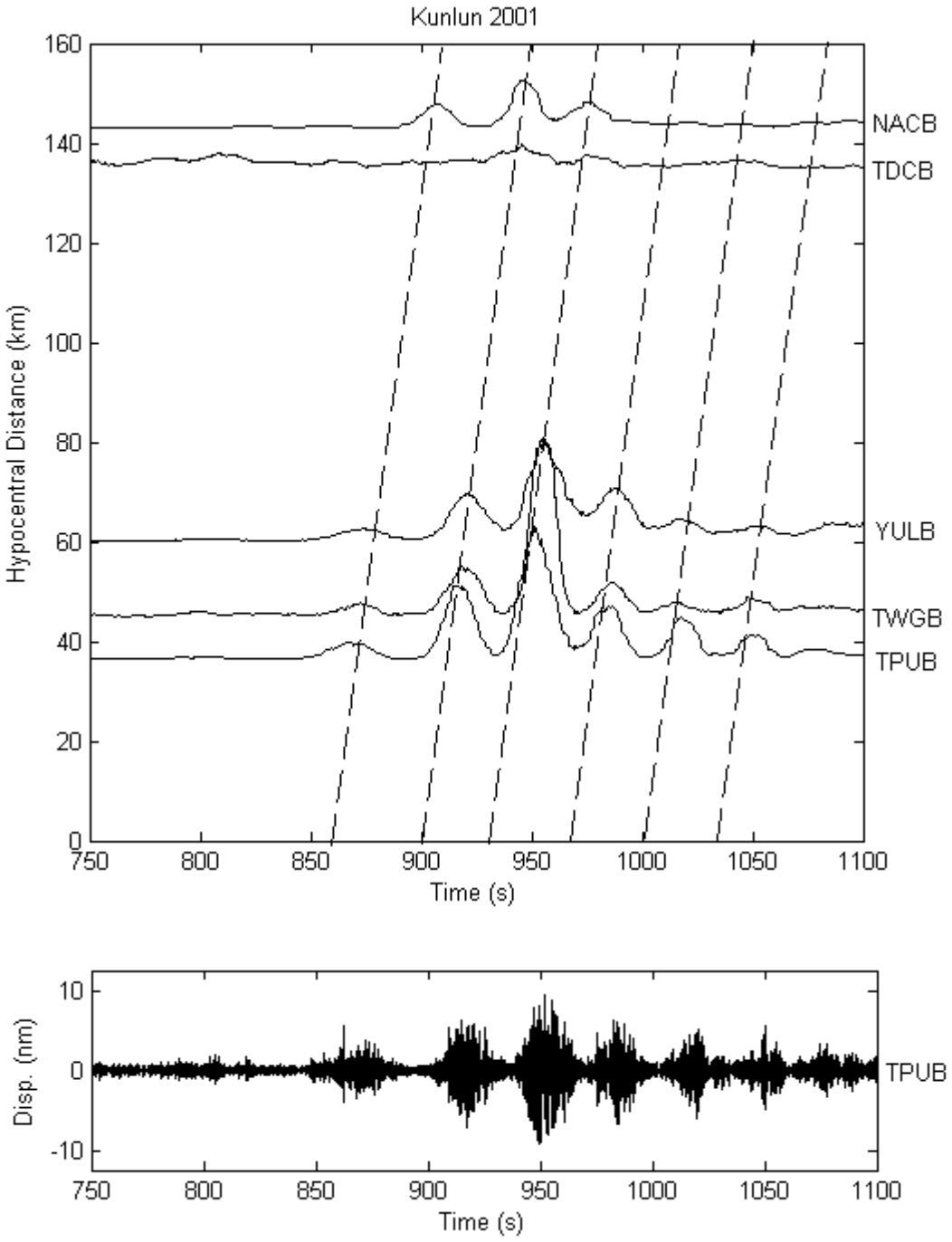
Kunlun 2001
Hypocentral Distance (km)
160
140
120
100
80
60
40
20
0
NACB
TDCB
YULB
TWGB
TPUB
750
800
850
900
950
1000
1050
1100
Time (s)
Disp. (nm)
10
0
-10
TPUB
Time (s)

Figure 3.3(a)

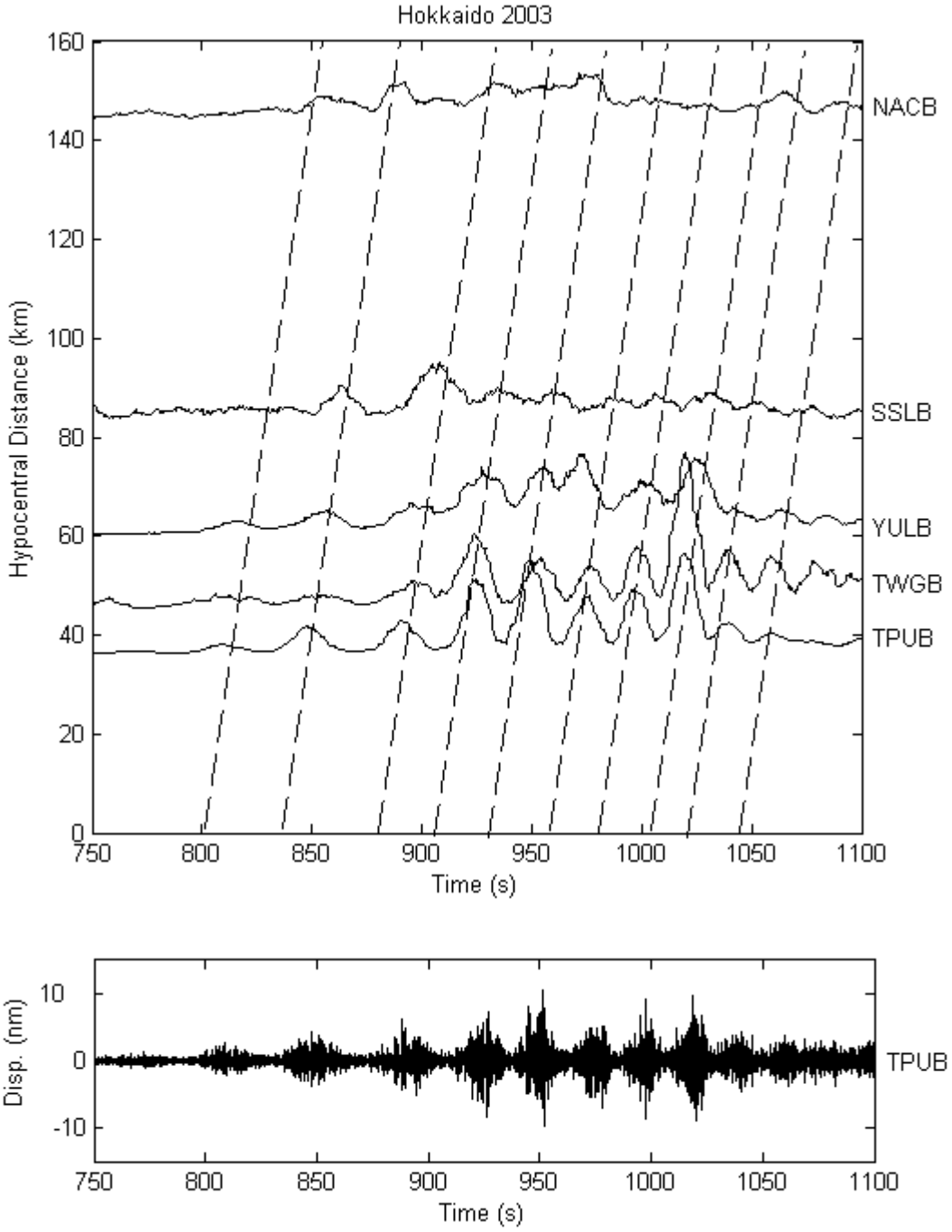
Hokkaido 2003
Hypocentral Distance (km)
160
140
120
100
80
60
40
20
0
NACB
SSLB
YULB
TWGB
TPUB
750
800
850
900
950
1000
1050
1100
Time (s)
Disp. (nm)
10
0
-10
TPUB
750
800
850
900
950
1000
1050
1100
Time (s)

Figure 3.3(b)

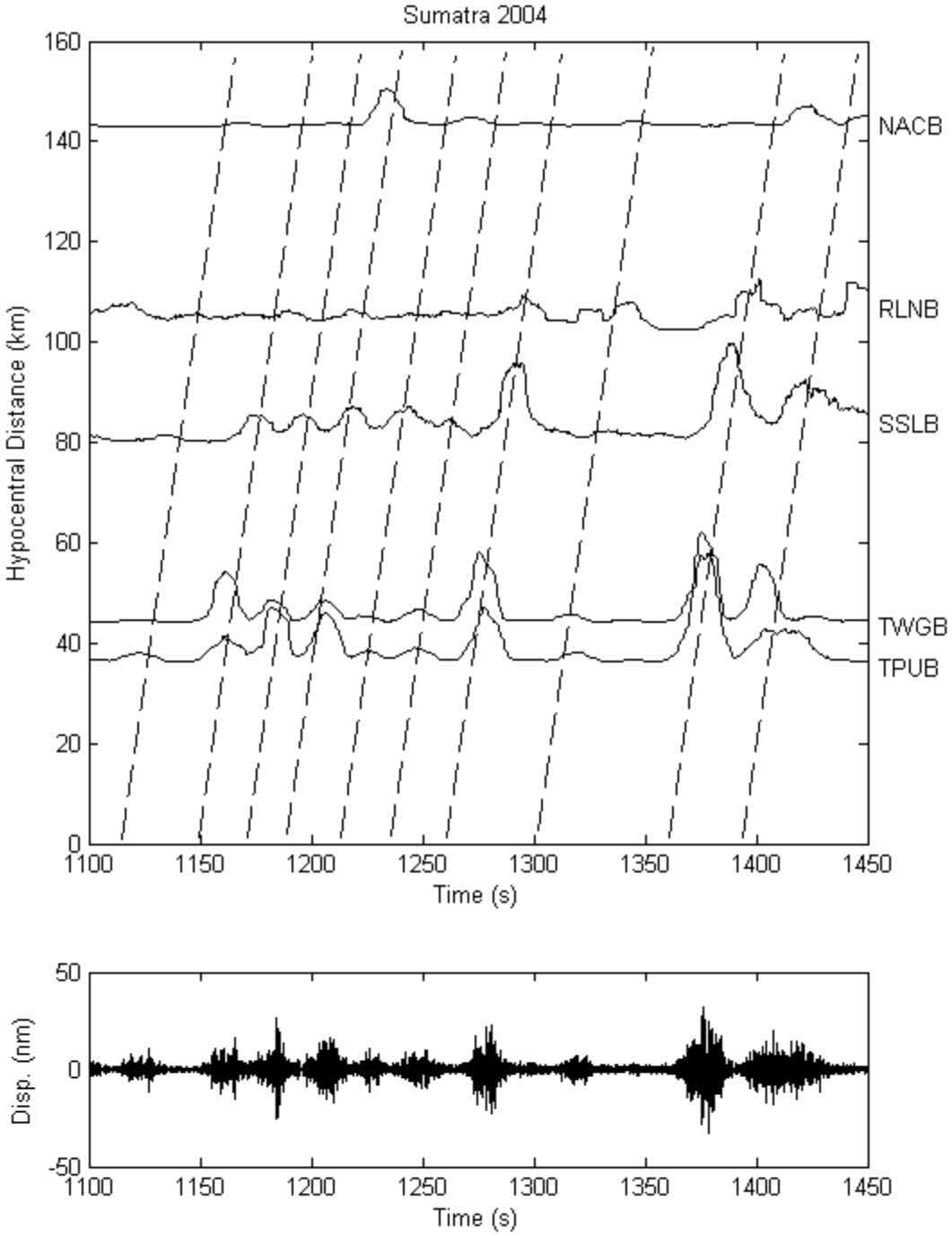
Sumatra 2004
Hypocentral Distance (km)
160
140
120
100
80
60
40
20
0
NACB
RLNB
SSLB
TWGB
TPUB
1100
1150
1200
1250
1300
1350
1400
1450
Time (s)
Disp. (nm)
50
0
-50
1100
1150
1200
1250
1300
1350
1400
1450
Time (s)

Figure 3.3(c)

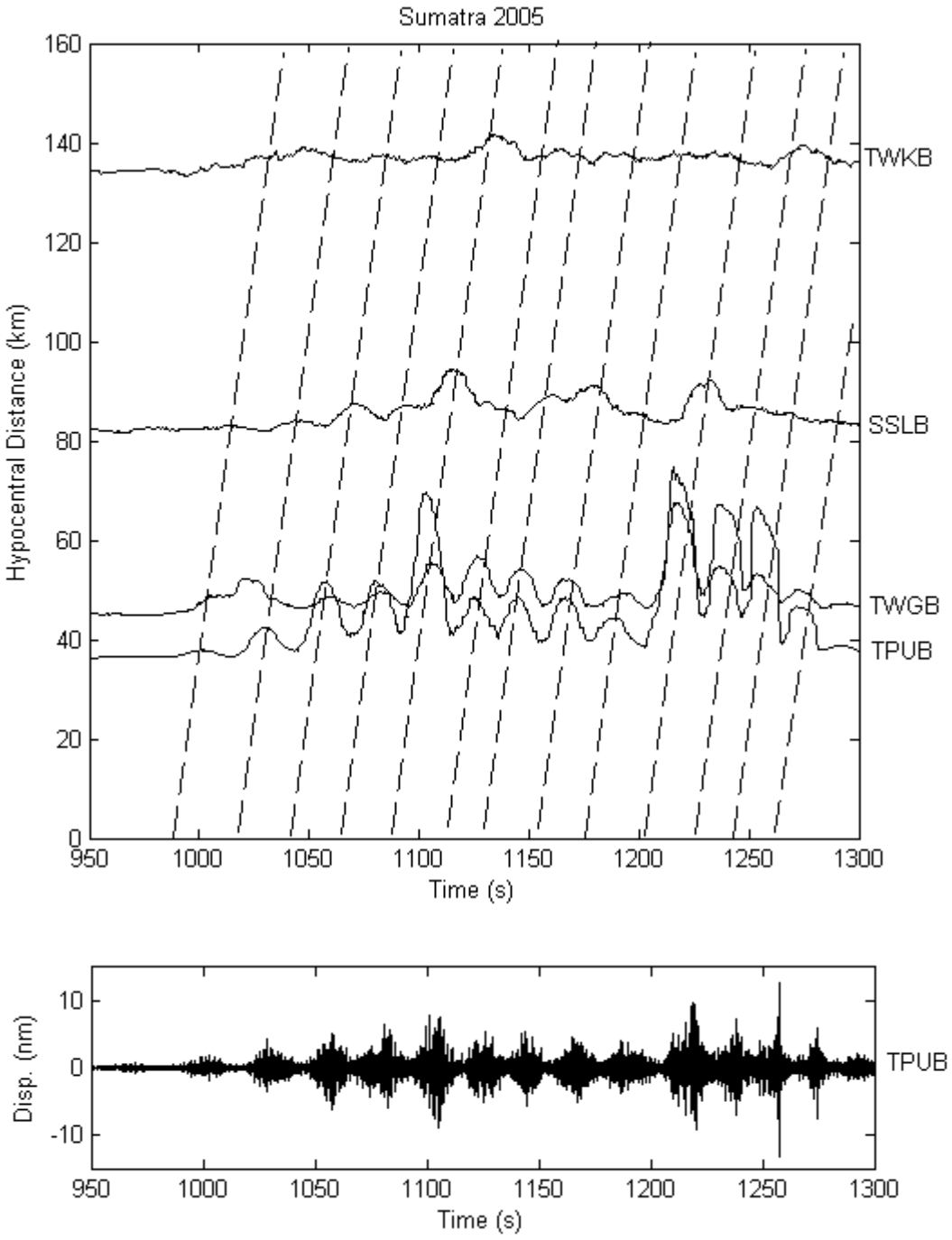
Sumatra 2005
Hypocentral Distance (km)
160
140
120
100
80
60
40
20
0
950
1000
1050
1100
1150
1200
1250
1300
Time (s)
TWKB
SSLB
TWGB
TPUB
Disp. (nm)
10
0
-10
TPUB
Time (s)

Figure 3.3(d)

Figure 3.3. Record sections of envelope functions showing the move-out of the tremor signal triggered by four large earthquakes: 2003 Mw 8.1 Hokkaido (a), 2001 Mw 8.1 Kunlun (b), 2004 Mw 9.2 Sumatra (c), and 2005 Mw 8.5 Sumatra (d). The dashed lines mark the S-wave (tremor velocity) travel time based on a 1D velocity model (Chen et al., 2001). Lower panels show the tremor as observed at the nearest station (TPUB).

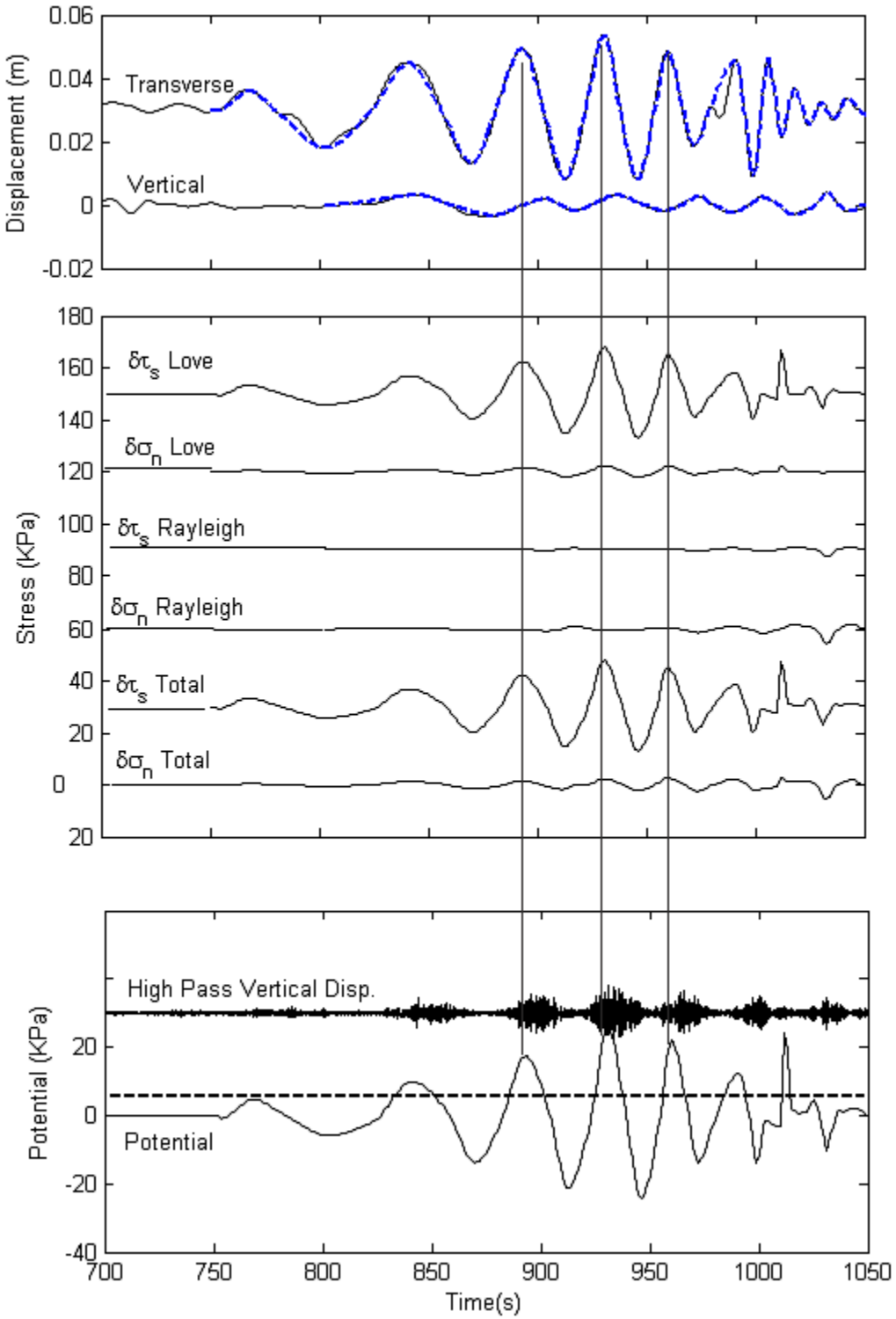

Figures 3.4 Top panel – Transverse and vertical displacements caused by passing of the Love and Rayleigh waves (respectively) caused by the 2001 Mw 7.8 Kunlun, China

earthquake at TPUB station. Blue dashed lines represent the synthetic displacements used to calculate stress. Middle panel – From top to bottom, changes in the shear ($\delta\tau_s\,Love$) and normal ($\delta\sigma_n\,Love$) stress caused by the Love wave; changes in the shear ($\delta\tau_s\,Rayleigh$) and normal ($\delta\sigma_n\,Rayleigh$) stress caused by the Rayleigh wave; and total change in the shear ($\delta\tau_s\,Total = \delta\tau_s\,Love + \delta\tau_s\,Rayleigh$) and normal ($\delta\sigma_n\,Total = \delta\sigma_n\,Love + \delta\sigma_n\,Rayleigh$) stress. Lower panel – Shows the triggering potential P as defined by equation 1 calculated with the total stress change and a μ=0.1, suggested threshold of 2 kPa for the triggering of NVT (dashed line), and 5 Hz high pass filtered vertical displacement revealing the NVT. In this case, shear stress caused by the Love waves seems to be the responsible for triggering (as describe in Figure 3.5).

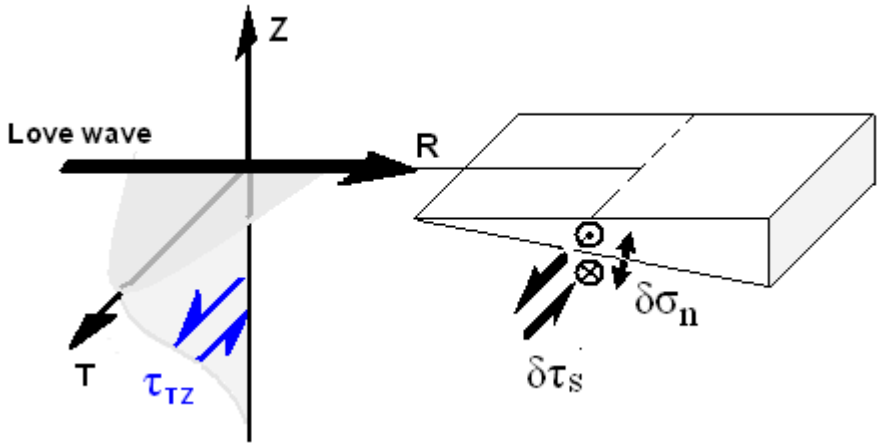

Figures 3.5 Triggering mechanism proposed for the 2001 Mw 7.8 Kunlun earthquake. In this cases, stress modeling shows a large contribution of Love wave to the local shear stress (Figure 3.6). Figure shows Love vertical (*Z*) and radial (R) direction of propagation. Love wave related stress component τ_{TZ} caused by the decrease in displacement with depth, acts in approximately the same direction as the fault local shear stress (strike direction as defined by circle symbols) adding shear stress ($\delta\tau_s$) in this direction and promoting sliding.

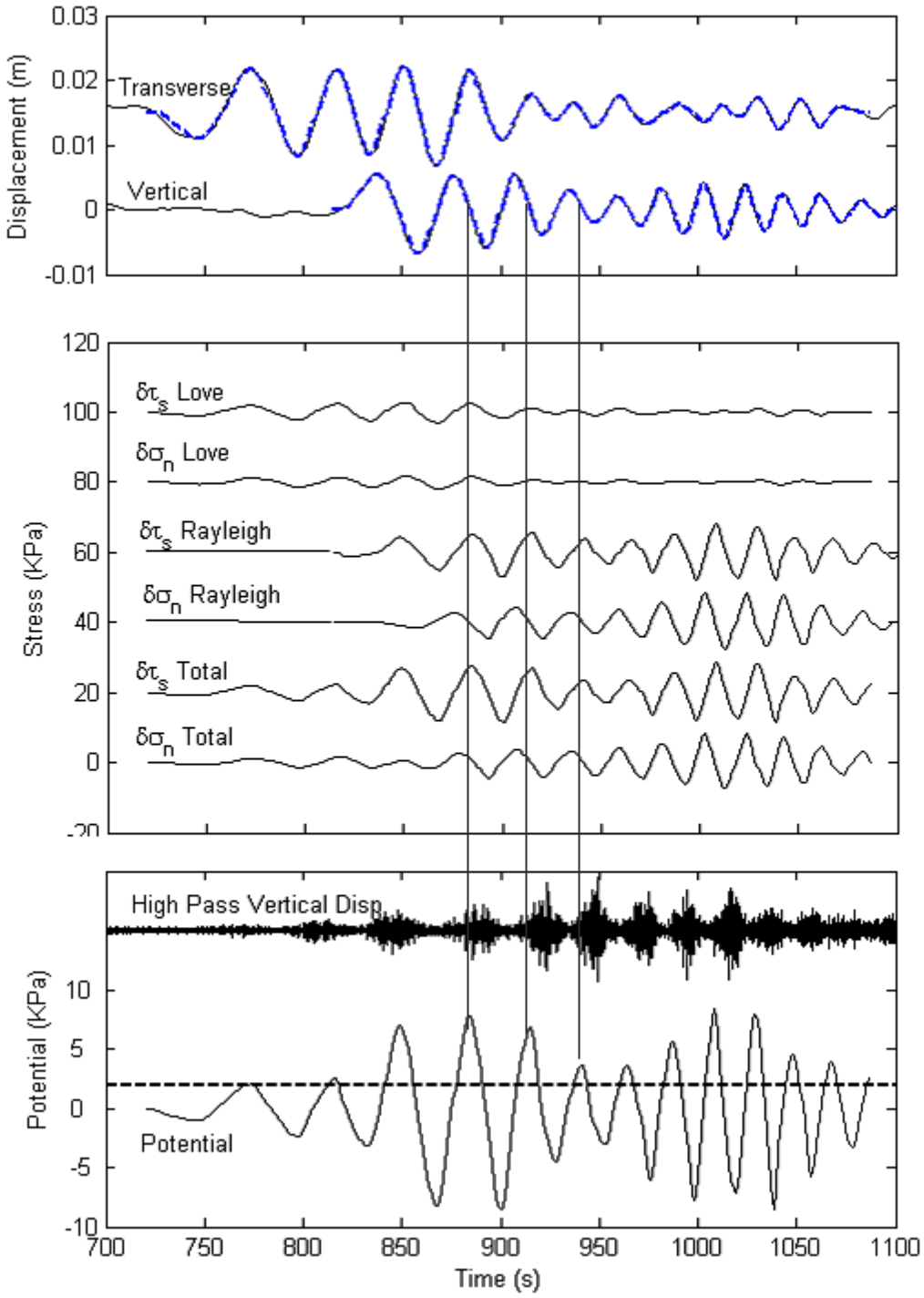

Figures 3.6 Top panel – Transverse and vertical displacements caused by passing of the Love and Rayleigh waves (respectively) caused by the 2003 Mw 8.3 Hokkaido,

Japan earthquake at station TPUB. Blue dashed lines represent the synthetic displacements used to calculate stress. Middle and lower panels, same as shown in figure 3.4. In this case, shear stress caused by the Rayleigh waves seems to be the responsible for triggering (see text for details).

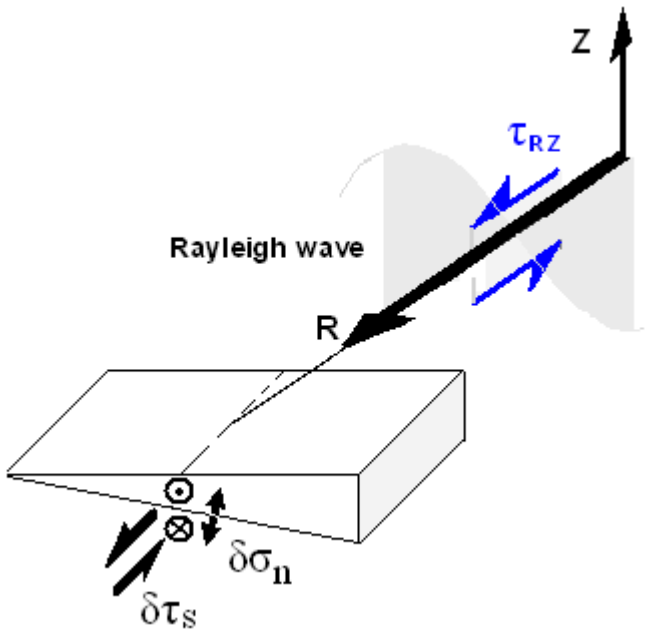

Figures 3.7 Triggering mechanism proposed for the 2003 Mw 8.3 Hokkaido, Japan earthquake. In this cases stress modeling shows a large contribution of Rayleigh wave to the local shear stress (Figure 3.6). Figure shows the Rayleigh wave vertical (*Z*) and radial (R) direction of propagation. Because the Rayleigh wave arrives almost parallel to the fault plane strike, the Rayleigh wave stress component, τ_{RZ} , acts in approximately the same direction as the fault local shear stress (strike direction as defined by circle symbols), adding shear stress ($\delta\tau_s$) in this direction and promoting sliding.

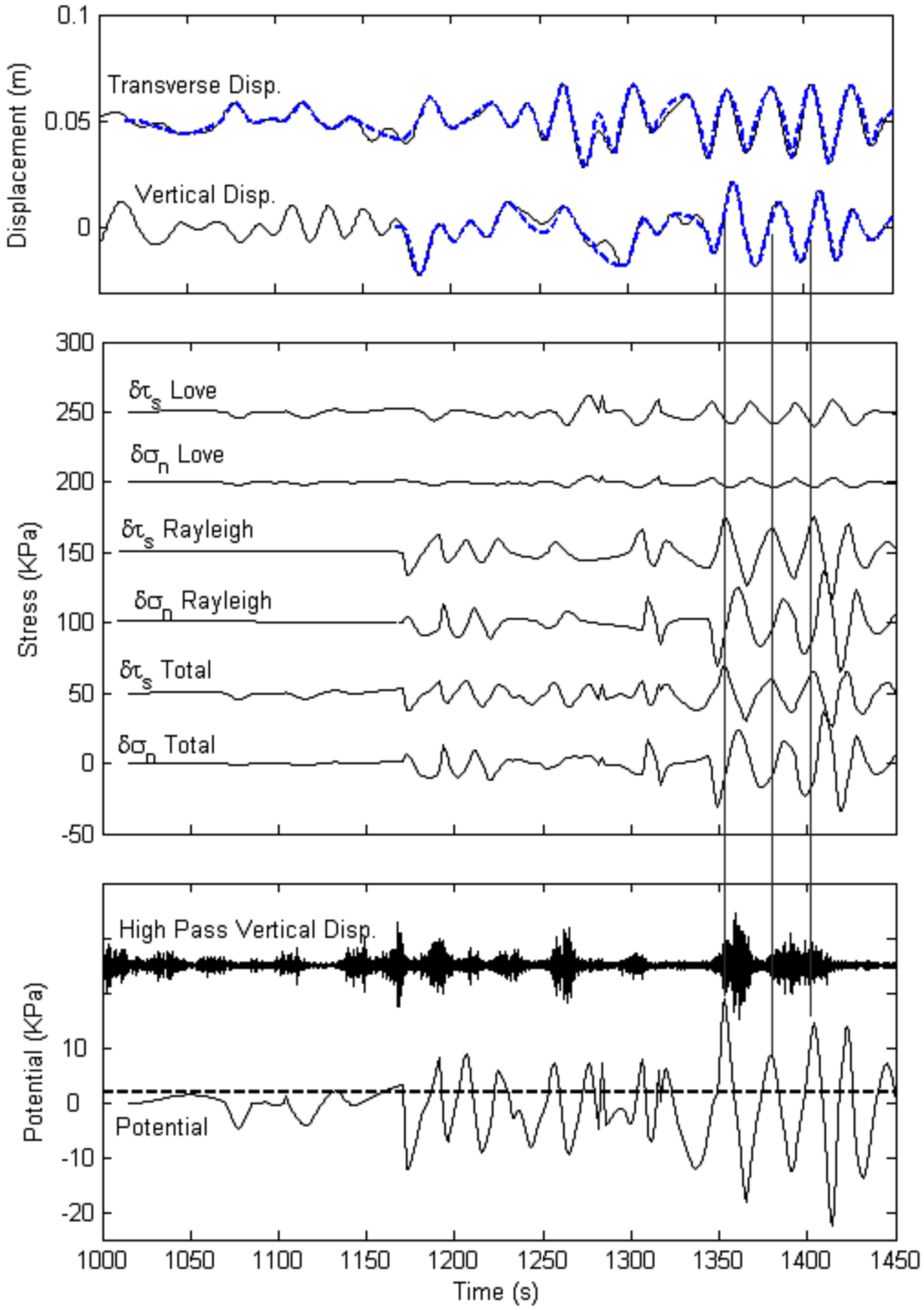

Figures 3.8 Top panel – Transverse and vertical displacements caused by passing of the Love and Rayleigh waves (respectively) caused by the 2004 Mw 9.0 Sumatra-Andaman earthquake at station TPUB. Blue dashed lines represent the synthetic

displacements used to calculate stress. Middle and lower panels, same as shown in figure 3.4. In this case, shear stress caused by the Rayleigh waves seems to be the responsible for triggering (as describe in Figure 10).

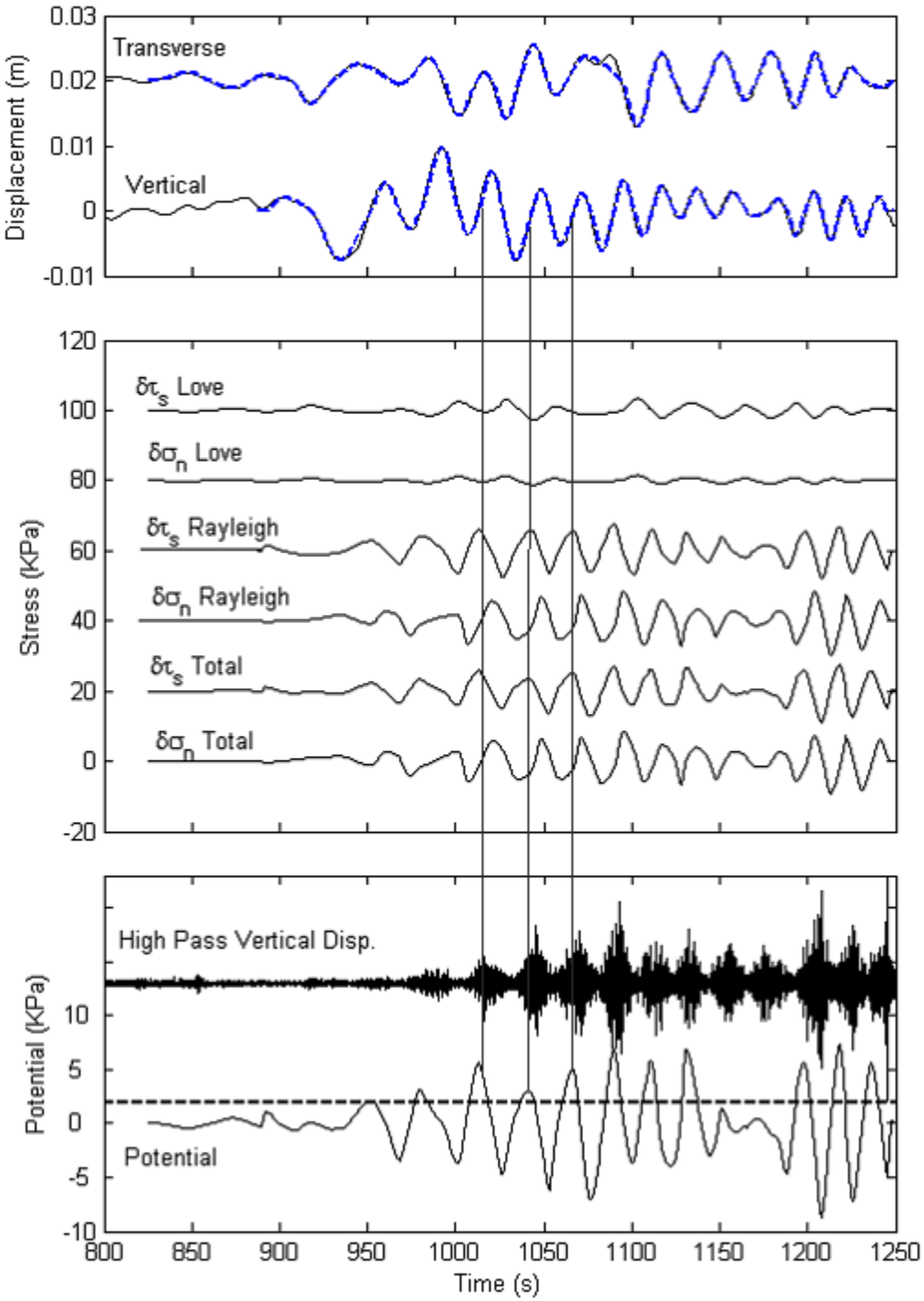

Figures 3.9 Top panel – Transverse and vertical displacements caused by passing of the Love and Rayleigh waves (respectively) caused by the 2005 Mw 8.7 Sumatra–Indonesia earthquake at TPUB station. Blue dashed lines represent the synthetic

displacements used to calculate stress. Middle and lower panels, same as shown in figure 3.4. In this case, shear stress caused by the Rayleigh waves seems to be the responsible for triggering (as describe in Figure 3.10).

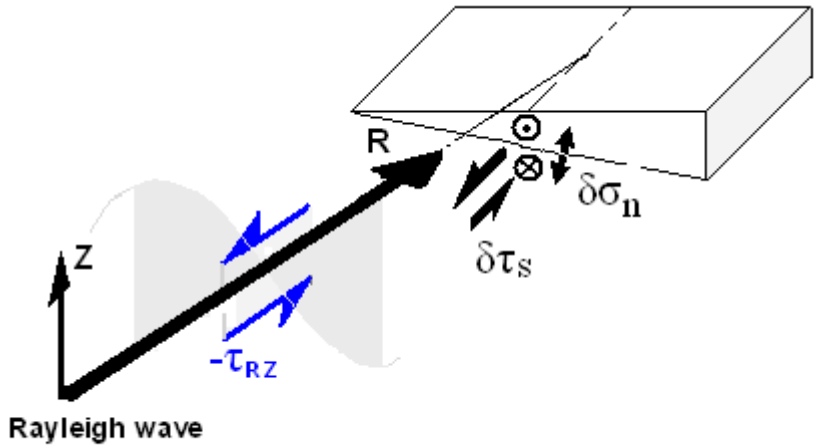

Figures 3.10 Figure shows the Rayleigh wave vertical (*Z*) and radial (R) direction of propagation. In this case stress modeling shows a high contribution of the Rayleigh wave to the local shear stress. This contribution $\delta\tau_s$ to the local shear stress (strike direction as defined by circle symbols) can account for the Rayleigh wave related shear stress component τ_{RZ} , promoting sliding.

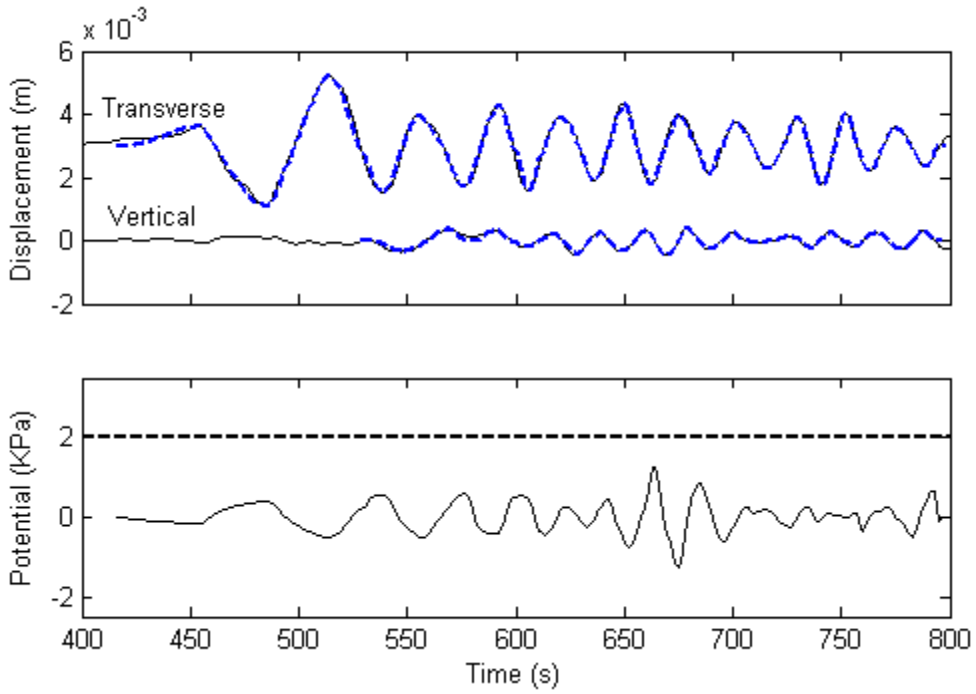

Figure 3.11(a)

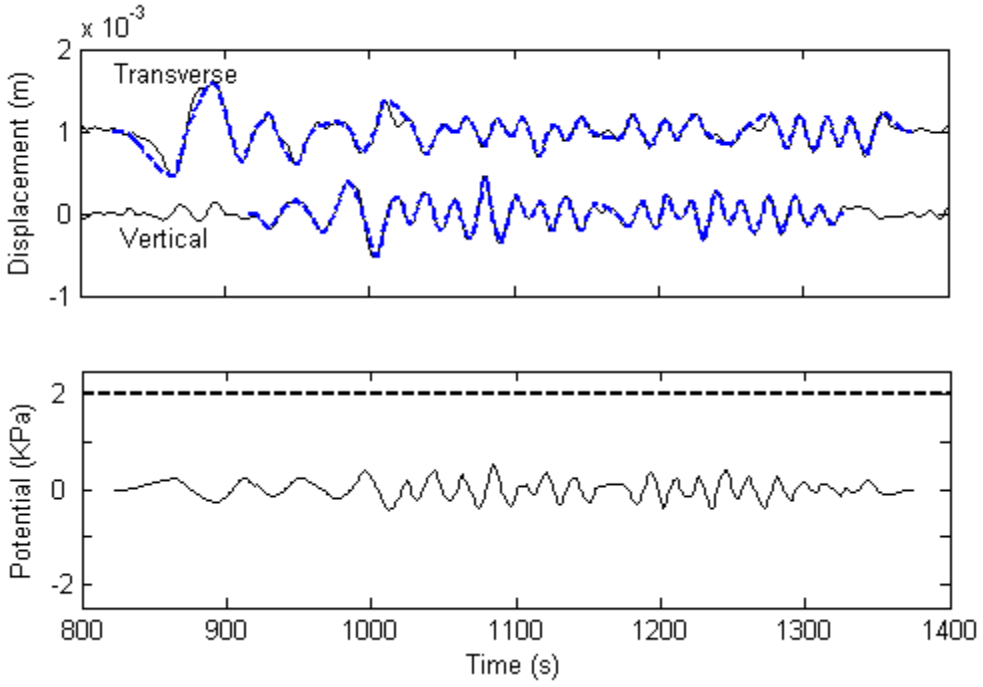

Figure 3.11(b)

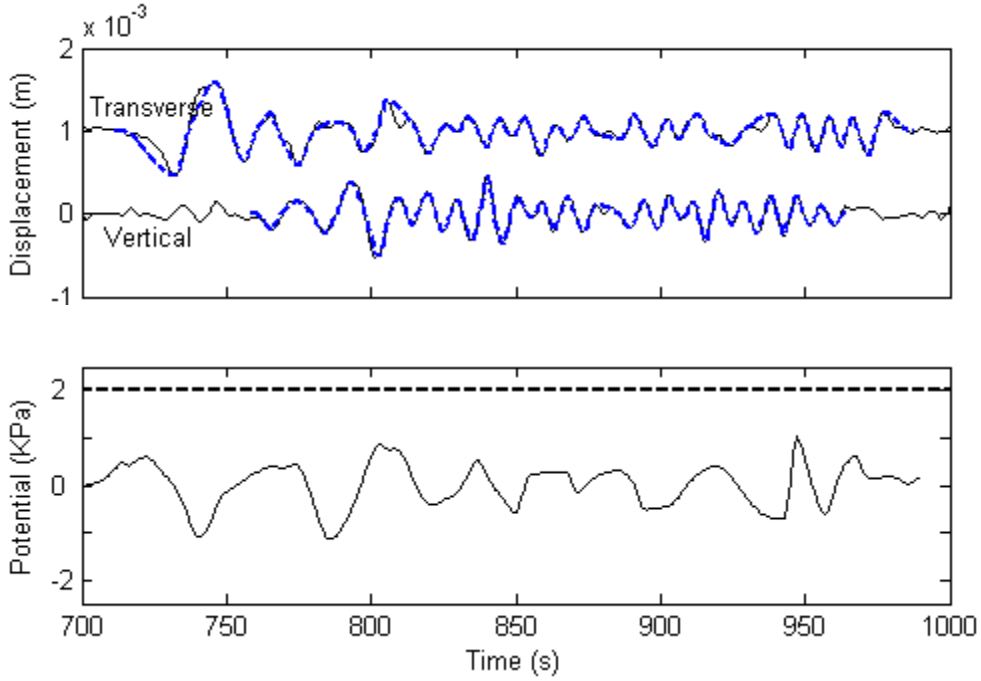

Figure 3.11(c)

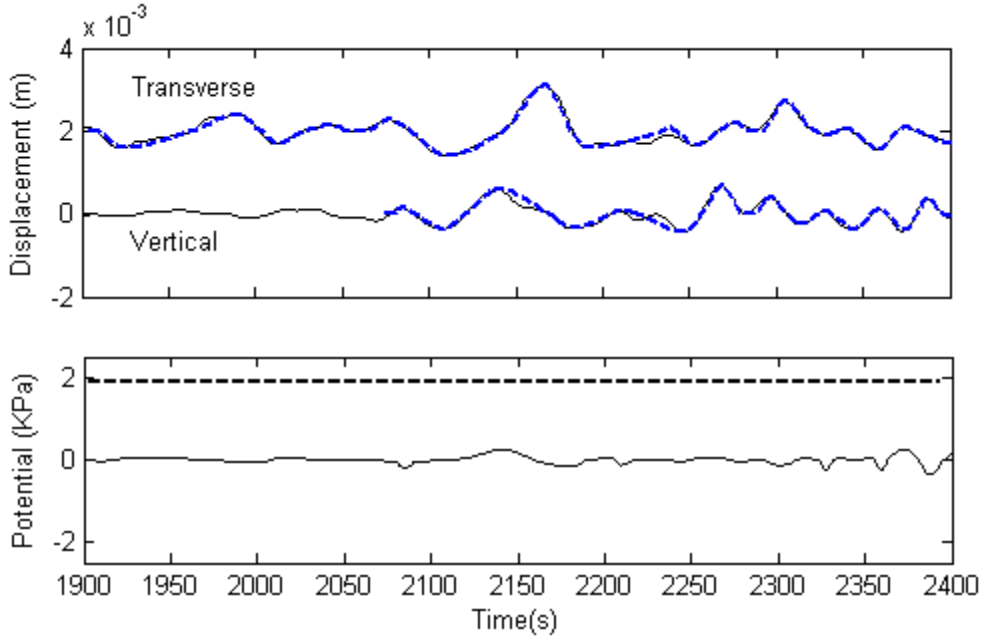

Figure 3.11(d)

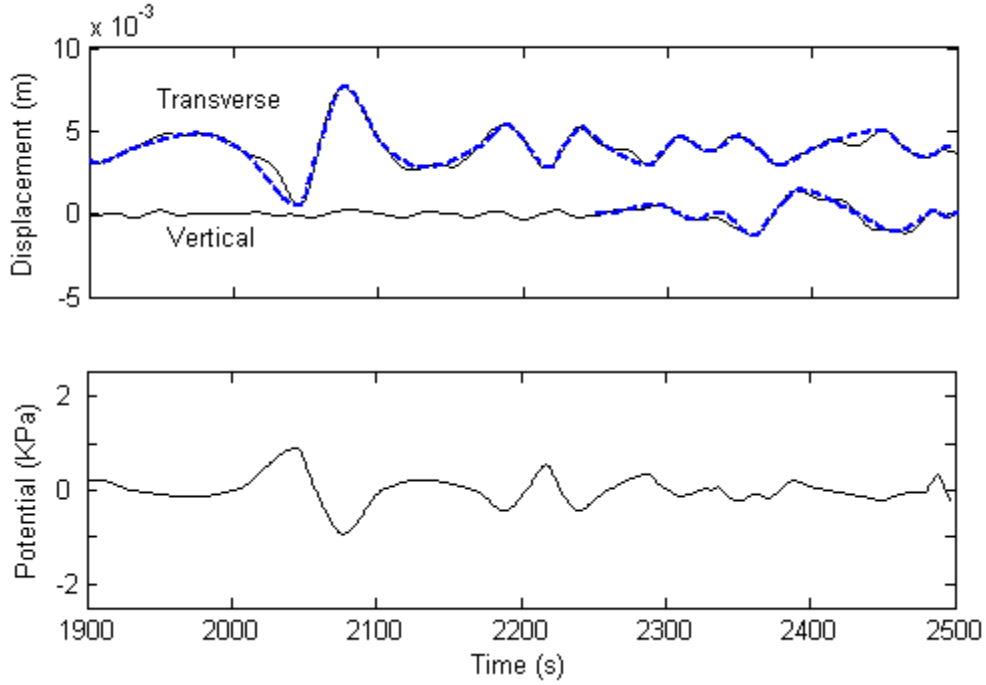

Figure 3.11(e)

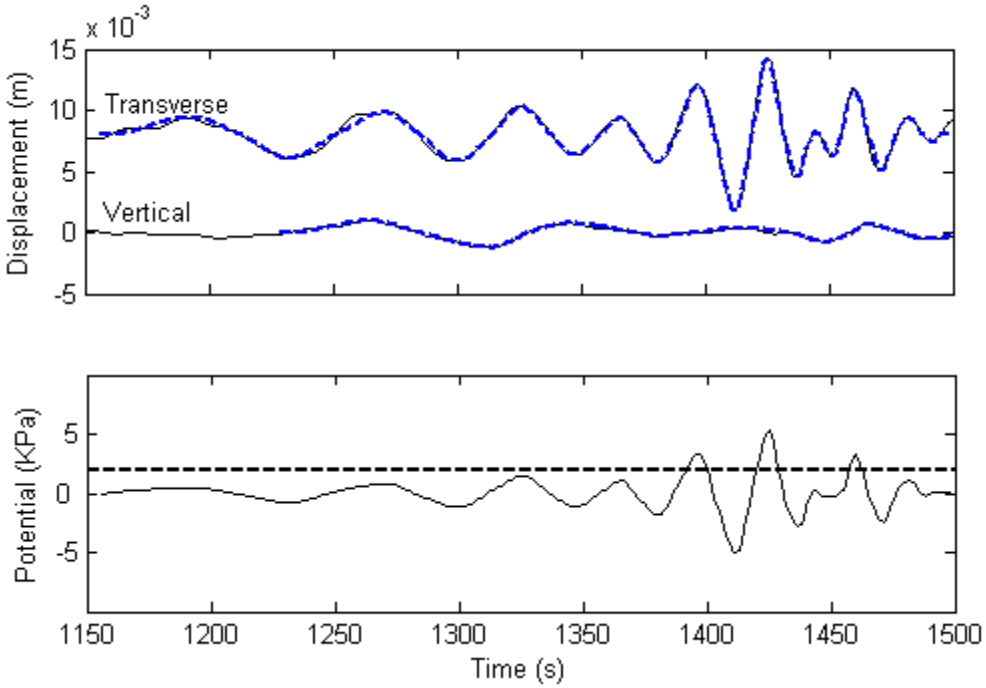

Figure 3.11(f)

Figure 3.11 Top panel shows the transverse and vertical displacements caused by passing of the Love and Rayleigh waves (respectively) for the non-triggering events: The 2002 Mw 7.5 Mindanao earthquake (a), the 2002 Mw 7.6 New Guinea earthquake (b), the 2002 Mw 7.5 Irian, Jaya, Indonesia earthquake (c), the 2002 Mw 7.9 Denali Fault earthquake (d), 2004 Mw 8.1 Macquarie Ridge earthquake (e), and the 2005 Mw 7.6 Pakistan earthquake (f). Only in case (f) is the suggested triggered potential of 2 kPa, all other events cause stress smaller than this threshold.

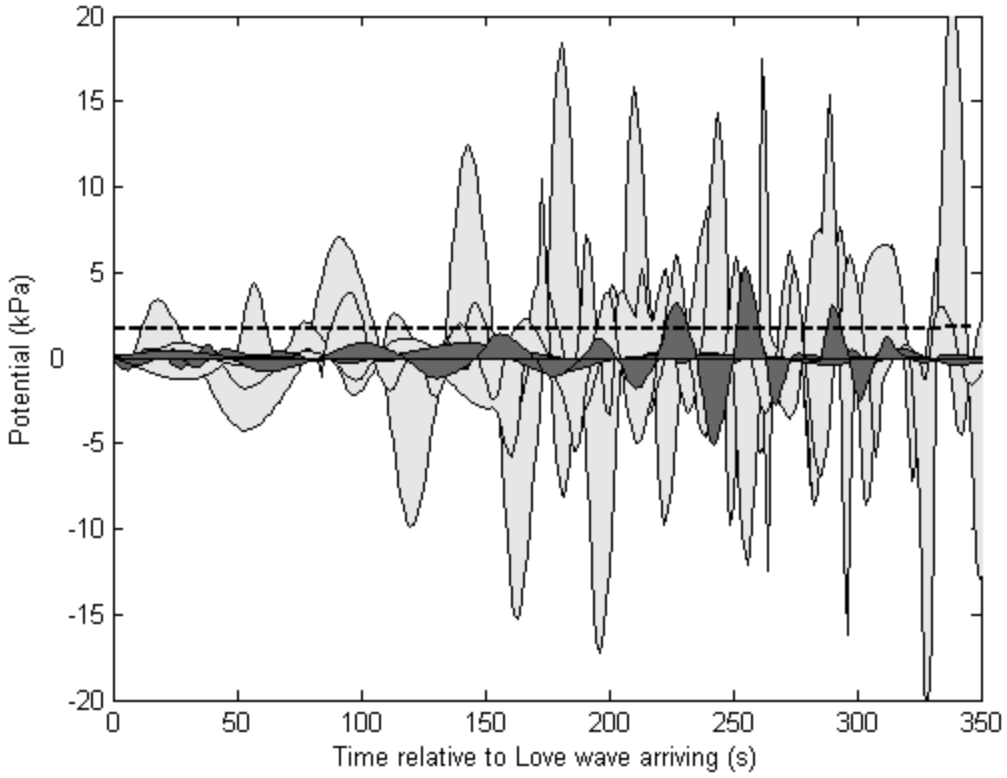

Figure 3.12 Overlap of the potentials for the ten events shifted relative to the arrival of Love waves. Dark colors represent the non-triggering events, while light color is for triggering events. In general, a threshold value for the triggering of tremors of 2 kPa describes our observations.

CHAPTER 4

DYNAMIC STRESS FOR TRIGGERED EVENTS IN UTAH FROM THE 1992 LANDERS AND THE 2002 DENALI EARTHQUAKES

4.1 ABSTRACT

Dynamic triggering occurs when the surface waves from large earthquakes change the stresses conditions on previously overstressed faults, promoting failure. In this study, we present our modeling of the dynamic stress that triggered two events in Utah, one triggered by the 1992 Landers earthquake and the other by the 2002 Denali Fault earthquake. The two triggered events show similar, well constrained, normal focal mechanisms. This allows a direct comparison of the normal and shear stress generated by the triggering events. We model the dynamic stress based on the particle motion of the Rayleigh and Love waves, which we rotate to the triggered fault plane to quantify the normal and shear stress. The change in the Coulomb stress function is calculated to compare the triggering potentials of the two large events. We show how dynamic stress modeling can be used to discriminate between the two axial planes of a first motion focal mechanism of a dynamically triggered event. We find that the waves from the Denali earthquake caused a change in the Coulomb stress about twice as large as the change caused by the Landers earthquake on a fault triggered by the Denali earthquake.

4.2 INTRODUCTION

According to the Elastic Rebound Theory (Reid, 1910), plate tectonic forces cause a gradual build up of stress, slowly distorting the crust of the Earth. Eventually, a fault cannot resist the strain any longer and fails. Studies have showed that secondary events such as Earth tides (Cochran et al., 2007), volcanic activity (Das and Scholz, 1981; Harris, 1998; Freed, 2005; Steacy et al., 2005), and other earthquakes (Hill et al., 1993; Anderson et al., 1994; Eberhart-Phillips et al., 2003; Gomberg et al., 2004; Husen et al., 2004; Pankow et al., 2004; Prejean et al., 2004; West et al., 2005; and Velasco et al., 2008), can add stress to a fault plane, triggering or promoting failure. Two of the most studied large earthquakes that triggered seismicity at large distance are the 28 June 1992 (M_w = 7.3) Landers, California earthquake (Hill et. al., 1993; Anderson et al., 1994; Bodin and Gomberg et al., 1994; Pankow et al., 2004) and the 3 November 2002 (M_w = 7.9) Denali Fault earthquake (DFE) (Gomberg et al., 2004; Husen et al., 2004; Husker and Brodsky et al., 2004; Prejean et al., 2004). Both earthquakes ruptured strike-slip faults and both had significant directivity that strongly impacted the surface wave amplitude in the directions of rupture (Velasco et al., 1992; Velasco et al., 2004). Seismicity caused by the Landers earthquake seemed to occur preferentially in regions of magma-related geothermal fluid flow or recent volcanic activity (Hill et al., 1993; Gomberg et al., 2001; Glowacka et al., 2002), while seismicity triggered by the DFE does not correlate with volcanic or geothermal activity (Gomberg et al., 2004). However, Velasco et al., (2008) showed that dynamic triggering is a global phenomenon, independent of the tectonic region or geothermal environment.

Both the Landers and the DFE triggered seismicity in Utah (Pankow et al., 2004). The DFE triggered a M 3.0 event near Salt Lake City, and the Landers earthquake triggered a M 4.0 event near Cedar City (Pankow et al., 2004). Figure 4.1 shows the location of the two triggered

events in Utah (Pankow et al., 2004) and the location of the seismic stations used for this study. Inset show location of the DFE and Landers earthquakes. To identify triggered events hidden in the wave trains of large earthquakes, a high pass filter is applied to broadband seismograms (Figure 4.1). As has been noted in other studies (e.g., Velasco et al., 2008), a time delay sometimes exists between the passage of the large amplitude surface waves and triggered events. Regardless, measuring the contribution that the surface waves generated by these large events have in the triggered fault's stress field can help us to understand the stress conditions are necessary for an earthquake to occur.

Generally, Peak Dynamic Stress (PDS), which is a proportionality of the recorder peak particle velocity, is used to measure triggering dynamic stress. Although this is useful for understanding overall stress conditions, this one-dimensional value cannot quantify the real change in the stress conditions on a triggered fault plane. This is because PDS is measured at the surface, and no assumptions are made about the depth at which triggering occurs. Furthermore, the change in stress conditions on a fault plane caused by a seismic wave is dependent on the orientation of the plane relative to the direction of wave propagation, factors that are not inferred from PDS measurements. In this study, we take the approach developed in Chapter 2 to model the stress change caused by the passing of surface waves to closely investigate the two triggered normal faults in Utah triggered by the DFE and the Landers earthquake. We found that the waves from the DFE caused a change in the Coulomb stress that was about twice as large as the change caused by the Landers earthquake on the possible fault plane triggered by DFE.

4.3 DYNAMIC STRESS MODELING

According to the Coulomb criterion, sliding on a fault plane will be promoted when an external event adds stress in the direction of the fault local shear stress, and/or in the normal direction to the fault plane, unclamping the fault and facilitating shearing. For example, in our case study, the triggering mechanism is normal, therefore, if the passing of surface waves causes a change in the dip direction, say $+\delta\tau_d$, and/or in the normal direction unclamping the fault, say $+\delta\sigma_n$, sliding will be promoted. In such a case, we can define the triggering potential by the change in the Coulomb failure function (Chapter 2):

$$Potential = \Delta CFF = \delta\tau_d + \mu\delta\sigma_n \quad (1)$$

which will be positive when failure is promoted (where μ is known as the coefficient of internal friction). The aim is to calculate the magnitude and orientation of the change in the fault plane shear and normal stress caused by the passing of the surface waves.

Dynamic stress can be calculated based on the particle motion of the Rayleigh and Love waves as a function of depth, wave frequency and amplitude at the surface, and elastic properties of the media (Chapter 2). In general, the Rayleigh waves' related maximum stress components are normal stresses (compression/dilatation) in the radial direction τ_{RR} and in the vertical direction τ_{ZZ}, and the shear stress τ_{RZ} (where Z represents for vertical and R radial), while Love waves generate only shear stresses τ_{RZ} and τ_{TZ} (T represents transversal). These stress components are grouped into a dynamic stress tensor, which can be rotated to the fault plane to measure its contribution to the fault plane local shear and normal stress. This is done for both set of surface waves and for every peak and inflection point, and then a quadratic interpolation is performed to represent the total potential as function of time (Chapter 3).

4.4 STRESS MODELING AND OBSERVATIONS

The Landers and DFE exhibited both strike-slip mechanisms and they caused similar ground motion and comparable PDS (~0.20 MPa) in the Utah region (Figure 4.2). Both events triggered an earthquake with well defined normal focal mechanisms in this region (Pankow et al., 2004). We model the dynamic stress responsible for the triggering. Since we do not know which of the two possible axial planes defined by the first motion mechanism is the actual fault plane, the stress caused by the passing of the surface waves is calculated for both axial planes.

In figures 4.3 and 4.5 the upper beach ball represents the focal mechanism triggered by the DFE, whereas the lower beach ball represents focal mechanism triggered by the Landers earthquake. In each of these figures black beach ball represents the event triggered by the earthquake in inset. Figure 4.3 shows the maximum potentials caused by the passing of surface waves generated by the DFE on both focal mechanisms. These potentials and stress components are presented in figure 4.4 as a function of time. Similarly, figure 4.5 shows the maximum potentials caused by the passing of the surfaces waves generated by the Landers event, and figure 6 shows these potentials and stress components as a function of time.

4.4.1 EVENT TRIGGERED BY THE 2002 DENALI FAULT EARTHQUAKE

The event triggered by the DFE (upper beach ball in figures 4.3 and 4.5) occurred ten years after the passing of the surface waves from the Landers earthquake. Why this local event was not triggered by the Landers earthquake but was triggered by the DFE, even though the PDS in the region was essentially the same for both events? In addition to other factors, such as the increase/decrease in the tectonic stress accumulated during the ten years between the two large events, and the possible stress changes due to the occurrence of other large and small events near this region, one factor that could favor the DFE over Landers for the triggering of this event is

the orientation and magnitude of the stress generated by the surface waves relative to the plane fault orientation.

The surface waves generated by the DFE caused a triggering potential equal to 0.44 MPa for the plane dipping north or axial plane 1, and 0.62 MPa for the plane dipping south or axial plane 2 plane (Figures 4.3 and 4.4), whereas the surface waves generated by the Landers event caused a potential of 0.47 MPa for the plane 1 and 0.29 MPa for the plane 2 (Figures 4.5 and 4.6). Note that potential for plane 1 was higher for Landers than for the DFE, the event which triggered this mechanism. If we assume that the local static stress was almost the same in this region (no tectonic loading) during the passing of the waves from Landers and the DFE, we can argue that axial plane 1 is less likely to be the actual fault plane, because this plane had already previously experienced (during the Landers event) changes in the Coulomb stress (or potential) greater that those caused by the DFE without failing. In other words, if plane 1 was the real fault plane, and failure occurred because the stress caused by the DFE (Potential = 0.44 MPa) overcame a threshold value for failure, then failure should have happened previously at the passing of the waves from Landers which reached a higher stress value (Potential = 0.47 MPa). On the other hand, if plane 2 is the real fault plane, we can see that it was not triggered by Landers but by the DFE because the DFE caused about twice (Potential = 0.62 MPa) the potential caused by Lander (Potential = 0.29 MPa).

4.4.2 EVENT TRIGGERED BY THE 1992 LANDERS EARTHQUAKE

The even triggered by the Landers earthquake showed normal focal mechanism with one axial plane dipping west (plane 1) and the other dipping southeast (plane 2). The surface waves generated by the Landers event caused a triggering potential of 0.59 MPa for plane 1 and 0.29

MPa for plane 2 (Figures 4.5 and 4.6). Ten years later the waves generated by the DFE caused a potential of 0.49 MPa on plane 1 and 0.35 MPa on plane 2. Note that the Landers event caused a larger potential than the DFE for plane 1, and the DFE causes a larger potential than the Landers event for plane 2. Following the logic of the previous example, we might say that plane 1 is the real fault plane, since plane 2 underwent a potential caused by the DFE higher than the caused by the Landers event without showing seismicity. However, in this case is more difficult to make assumptions about which is the real fault plane. For example, it is possible that plane 2 was the real fault plane, so that the passing of the surface waves generated by the Landers event triggered failure in this plane releasing the accumulated local stress and that the stress build up on this fault plane by the time when the DFE occurred could be not large enough to be triggered by the DFE's surface waves. On the other hand, the magnitude of the potential caused by the Landers event on plane 1 (0.59 MPa) seems more consistent with the magnitude of the potential that we assume to have triggered seismicity for the DFE event (0.62 MPa).

4.5 DISCUSSION

By modeling the change in the normal and shear stress on a fault plane caused by dynamic stress, we can quantify more precisely the contribution of the distance event to the local stress responsible for failure. Even though the PDS can be used to estimate the change in the local stress, this change will be more related to planes orthogonal to the direction of wave propagation. Stress thresholds can be calculated by modeling a large number of triggering and non-triggering events acting on a fault plane. By quantifying the contribution in the local normal and shear stress direction, dynamic triggering seismicity can be use as an indicator of the fault strength.

Although the delay observed in triggered events related to the arriving triggering waves is difficult to explain using a frictional approach, a large change in the Coulomb stress represents the potential of a wave to cause strain in a system, which can result in damage to fault's contacts, and consequently the weakening of the fault, accelerating failure.

4.6 CONCLUSIONS

We analyzed the dynamic stress caused by the passing of the surfaces waves from two large events, the 1992 Landers earthquake and the 2002 DFE that triggered seismicity in Utah. We modeled the stress that triggered two of the largest dynamically triggered events in this region, both of which show a well-constrained normal fault mechanism. We showed how dynamic stress modeling can be used to discriminate between the axial planes of a first motion focal mechanism of a dynamically triggered event. In the case of the event triggered by the DFE, the axial plane dipping south (plane 2) seems to be real fault plane. For the event triggered by the Landers earthquake we cannot determine which is the real fault plane, however, the magnitude of the stress change observed for the west dipping plane (plane 1) is greater and more consistent with the amount of stress change in the first case study. The modeling of dynamic stress triggering constitutes an important tool for understanding the stress conditions under which earthquakes occur.

LIST OF REFERENCES

Anderson, J. G., J. N. Brune, J. N. Louie, Y. Zeng , M. Savage, G. Yu, Q. Chen, and D. de Polo (1994). Seismicity in the western Great Basin apparently triggered by the Landers, California, earthquake, *Bull. Seismol. Soc. America,* 84, 863-891.

Cochran, E. S., J. E. Vidale, and S. Tanaka (2004). Earth tides can trigger shallow thrust fault earthquakes, *Science,* 306, 1164– 1166.

Das, S. and Scholz, C. (1981). Off-fault aftershock clusters caused by shear stress increase? *J. Geophys. Res.*, 71, 1669-1675.

Eberhart-Phillips, D., Haeussler, P. J., Freymueller, J. T., Frankel, A. D., Rubin, C. M., Craw, P., Ratchkovski, N. A., Anderson, G., Carver, G. A., Crone, A. J., Dawson, T. E., Fletcher, H., Hansen, R., Harp, E. L., R.A., H., Hill, D. P., Hreinsdottir, S., Jibson, R. W., Jones, L. M., Kayen, R., Keffer, D. K., Larsen, C. F., S.C., M., Personius, S. F., Plafker, G., Sherrod, B., Sieh, K., Sitar, N. and Wallace, W. K. (2003). The 2002 Denali Fault earthquake, Alaska: a large magnitude, lippartitioned event, *Nature,* 300, 1113-1118.

Freed, A. M. (2005). Earthquake triggering by static, dynamic, and postseismic stress transfer *Ann. Rev. Earth Planet. Sci*., 33, 335-367.

Glowacka, E., A. F. Nava, D. Cossio, V. Wong, and F. Farfan (2002). Fault slip, seismicity, and deformation in the Mexicali Valley, Baja California, Mexico, after the M 7.1 Hector Mine earthquake *Bull. Seismol. Soc. America,* 92, 1290-1299.

Gomberg, J., P. Bodin, K. Larson, and H. Dragert, (2004). Earthquake nucleation by transient deformations caused by the M = 7.9 Denali, Alaska, earthquake, *Nature,* 427, 621-624.

Gomberg, J., P. A. Reasenberg, P. Bodin, and R. A. Harris (2001). Earthquake triggering by seismic waves following the Landers and Hector Mine earthquakes, *Nature*, 411, 462–466.

Harris, R. A. (1998). Introduction to a special section: Stress triggers, stress shadows, and implications for seismic hazards *J. Geophys. Res.*, 103, 24,347-24,358.

Hill, D. P., Reasenberg, P. A., Michael, A., Arabaz, W. J., Beroza, G., Brumbaugh, D., Brune, J. N., Castro, R., Davis, S., dePolo, D., Ellsworth, W. L., Gomberg, J., Harmsen, S., House, L., Jackson, S. M., Johnston, M. J. S., Jones, L., Keller, R., Malone, S., Munguia, L., Nava, S., Pechmann, J. C., Sanford, A., Simpson, R. W., Smith, R. B., Stark, M., Stickney, M., Vidal, A., Walter, S., Wong, V. and Zollweg, J. (1993). Seismicity remotely triggered by the magnitude 7.3 Landers, California, earthquake *Science*, 260, 1617-1623.

Husen, S., R.Taylor , R. B. Smith, and H. Healser, (2004). Changes in geyser eruption behavior and remotely triggered seismicity in Yellowstone National Park produced by the 2002 M 7.9 Delani fault earthquake, *Alaska Geology*, 32, 537-540.

Pankow, K. L., Arabasz, W. J., Pechmann, J. C. and Nava, S. J. (2004). Triggered seismicity in Utah from the 3 November 2002 Denali Fault earthquake *Bull. Seismol. Soc. America*, 94, S332-S347.

Prejean, S. G., D. P. Hill, Brodsky, E. E., Hough, S. E., Johnston, M. J. S., Malone, S. D., Oppenheimer, D. H., Pitt, A. M. and Richards-Dinger, K. B. (2004). Remotely triggered seismicity on the United States west coast following the Mw 7.9 Denali Fault earthquake *Bull. Seismol. Soc. America*, 94, S348-S359.

Reid, H. (1910). Permanent displacements of the grounds: *in* The California Earthquake of April 18, 1906, *Report of the State Earthquake Investigation Commission*, v. 2, Carnegie Institution of Washington, Washington, D.C., p. 16-32.

Steacy, S., J. Gomberg, and M. Cocco, (2005). Introduction to special section: Stress transfer, earthquake triggering, and time-dependent seismic hazard *J. Geophys. Res*., 110, doi:10.1029/2005JB003692.

Velasco, A. A., S. Hernandez, T. Parson and K. Pankow (2008). Global ubiquity of dynamic earthquake triggering, *Nature Geosciences*, 1, 375-379.

Velasco, A. A., C. J. Ammon, J. Farrell, and K. Pankow, (2004). Rupture directivity of the November 3, 2002 Denali fault earthquake determined from surface waves, *Bull. Seism. Soc. Am.*, 94, S293-S299.

Velasco, A. A., T. Lay, and J. Zhang, (1992). Improved resolution of earthquake source parameters from long-period surface wave inversions, *Phys. Earth Planet. Int.*, 74, 01-107.

West, M., J.J. Sanchez, and S.R. McNutt (2005). Periodically triggered seismicity at Mount Wrangell, Alaska, after the Sumatra earthquake, *Science*, 308, 1144-1146.

FIGURES

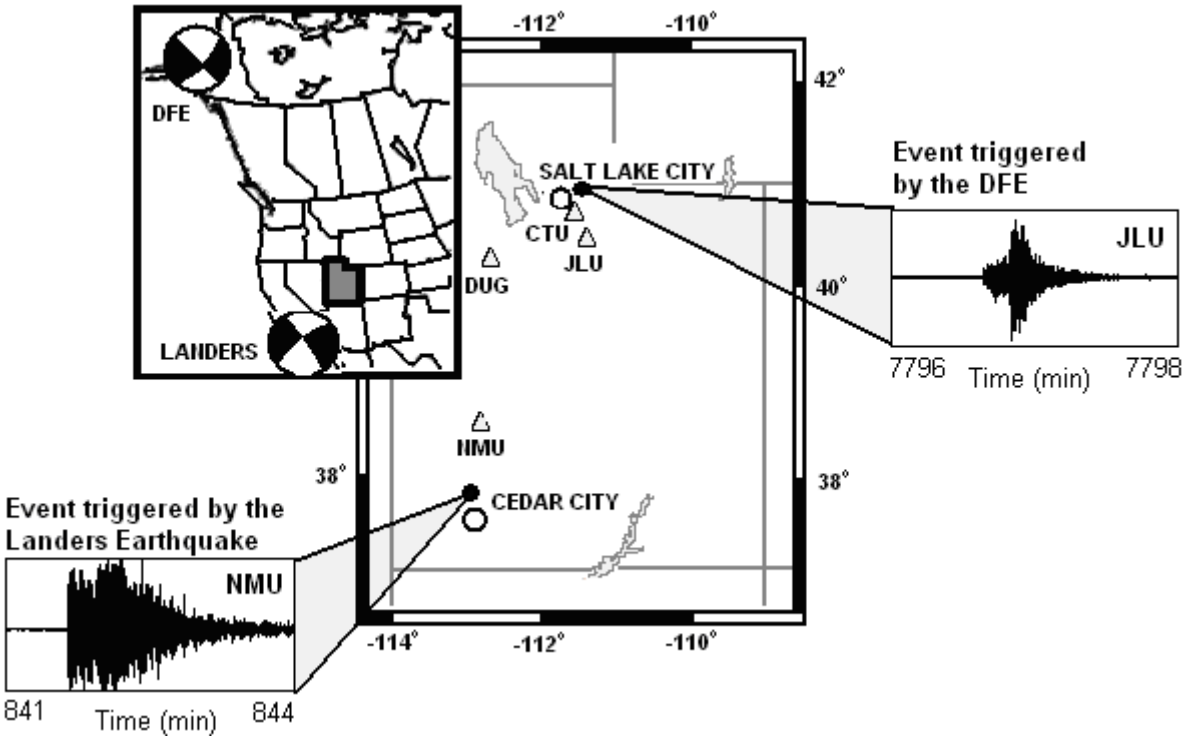

Figure 4.1. Map shows location of normal events triggered in Utah by the 2002 Denali Fault Earthquake (DFE) and the 1992 Landers earthquake and seismic stations used in this study (triangles). The Landers event triggered a M 4.0 with a delay of 0.55 days near Cedar City at a depth of 8.0 km. The DFE triggered a M 3.0 event with a delay of 4.6 days near Salt Lake City, at 7.4 km depth (Pankow et al., 2002). High pass filtered (at 5 Hz) vertical component seismograms from University of Utah seismic stations NMU and JLU show the triggered events. Inset shows location of the DFE and Landers earthquakes.

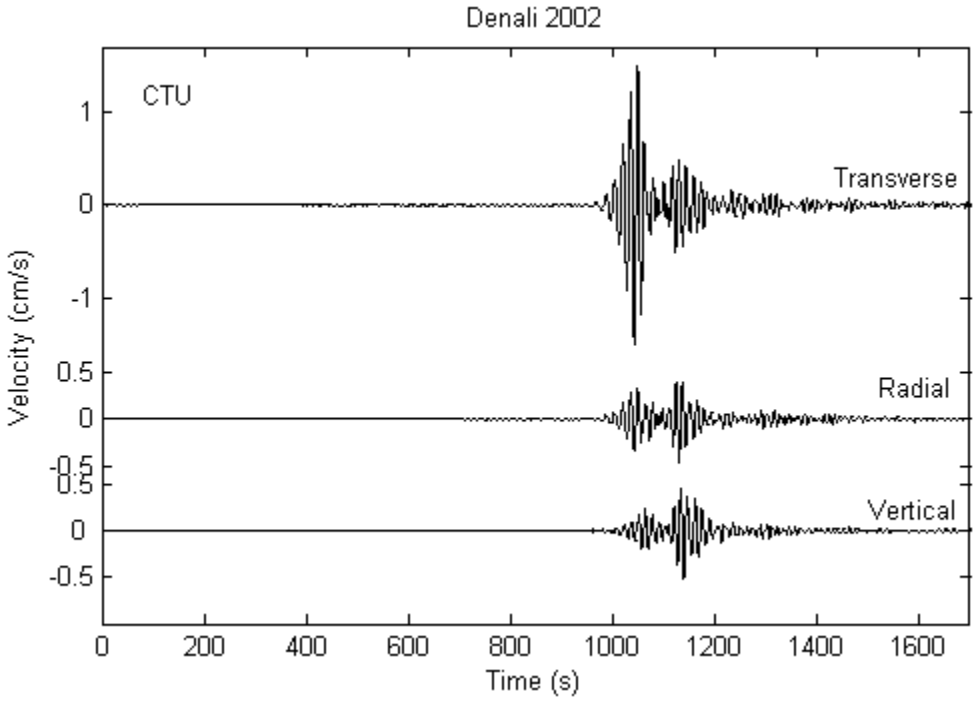

Figure 4.2(a)

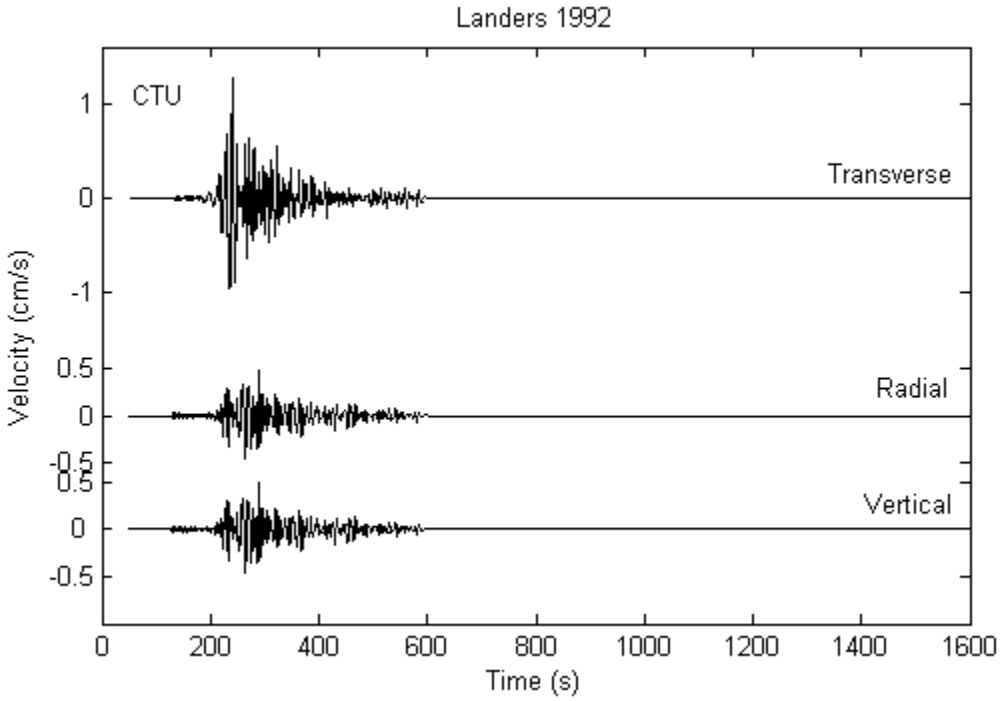

Figure 4.2(b)

Figure 4.2. Seismic waves as recorded by the three component DUG seismic station (see figure 4.1 for location). Transverse, radial and vertical components are showed for the DFE (a), and the Landers earthquake (b).

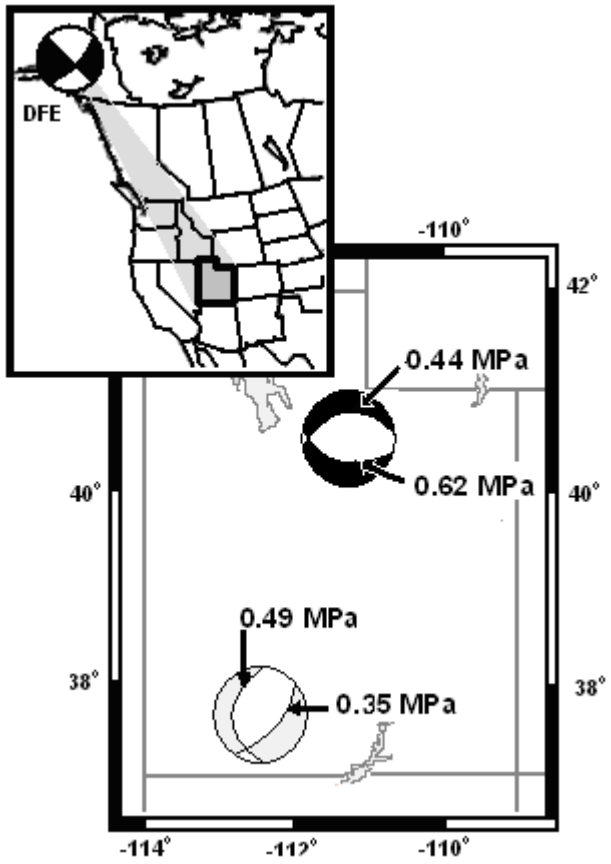

Figure 4.3. Black beach ball represents the earthquake triggered by the DFE and gray color beach ball represents the earthquake triggered by the Landers event. Triggering potentials for the surface waves generated by the DFE, on the two possible axial planes, are shown for each focal mechanism.

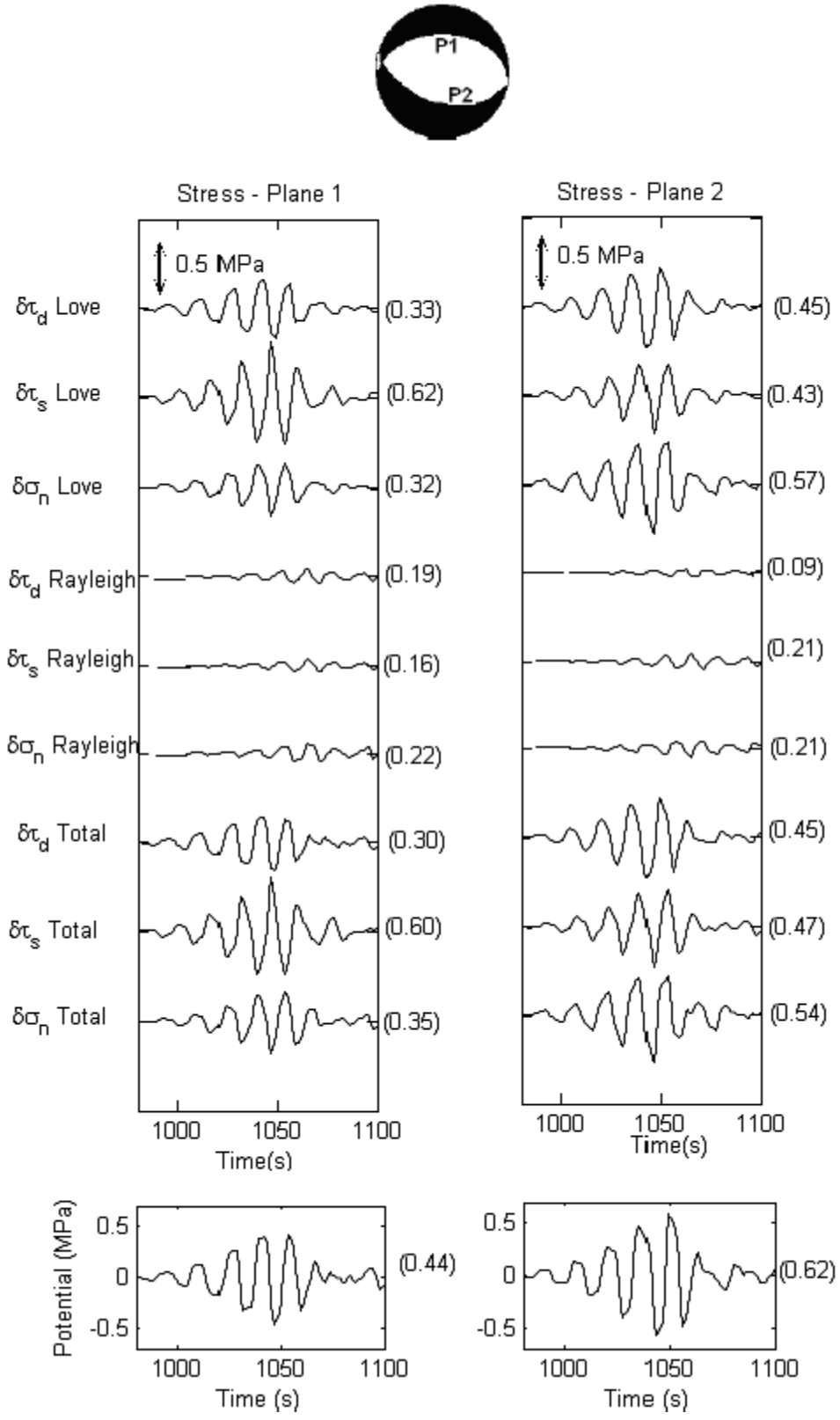
P1
P2
Stress - Plane 1
Stress - Plane 2
0.5 MPa
0.5 MPa
δτd Love
δτs Love
δσn Love
δτd Rayleigh
δτs Rayleigh
δσn Rayleigh
δτd Total
δτs Total
δσn Total
(0.33)
(0.62)
(0.32)
(0.19)
(0.16)
(0.22)
(0.30)
(0.60)
(0.35)
(0.45)
(0.43)
(0.57)
(0.09)
(0.21)
(0.21)
(0.45)
(0.47)
(0.54)
1000
1050
1100
Time(s)
Potential (MPa)
0.5
0
-0.5
(0.44)
(0.62)
Time (s)

Figure 4.4(a)

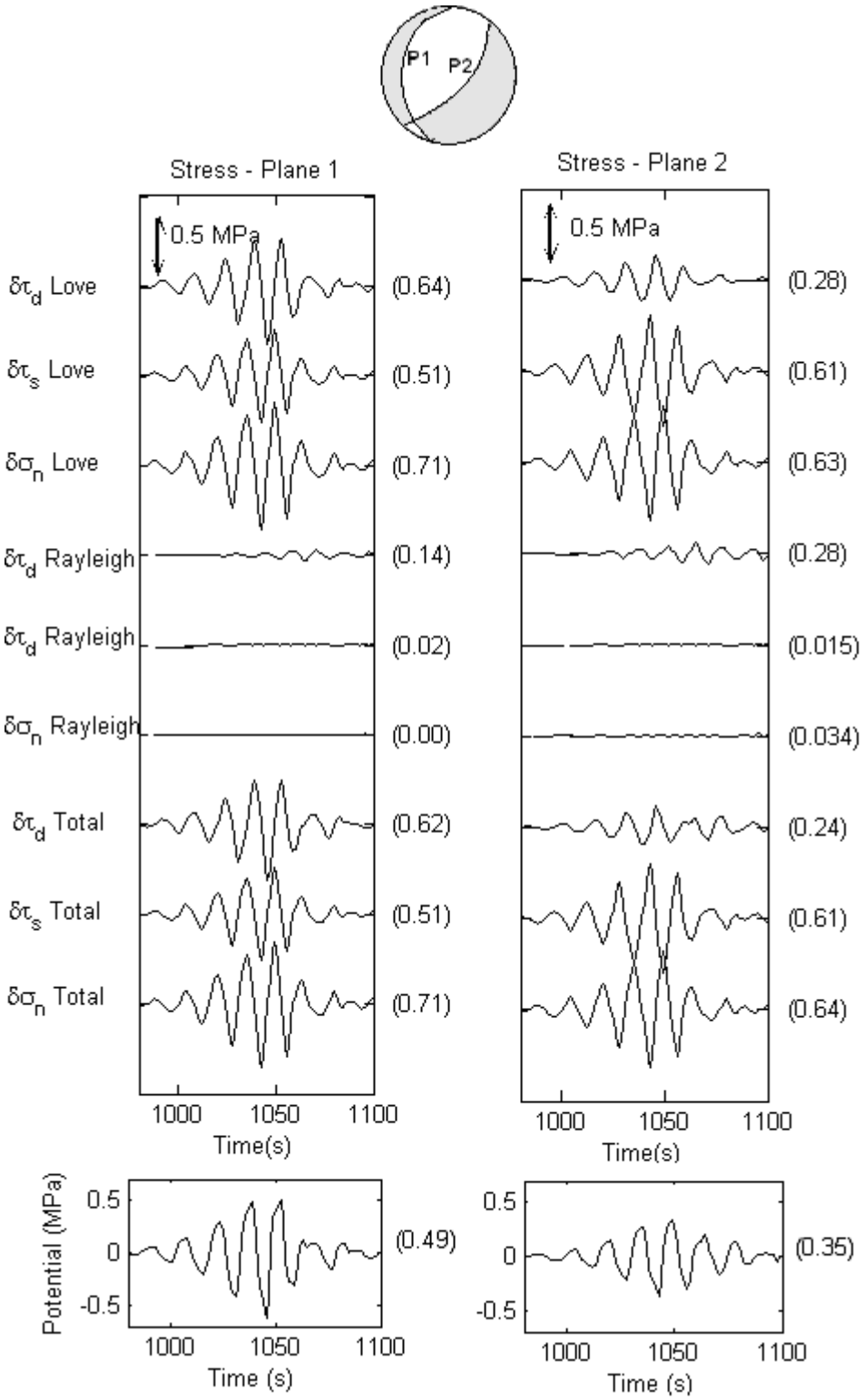
P1
P2
Stress - Plane 1
Stress - Plane 2
0.5 MPa
0.5 MPa
δτd Love
δτs Love
δσn Love
δτd Rayleigh
δτd Rayleigh
δσn Rayleigh
δτd Total
δτs Total
δσn Total
(0.64)
(0.51)
(0.71)
(0.14)
(0.02)
(0.00)
(0.62)
(0.51)
(0.71)
(0.28)
(0.61)
(0.63)
(0.28)
(0.015)
(0.034)
(0.24)
(0.61)
(0.64)
1000
1050
1100
Time(s)
Potential (MPa)
0.5
0
-0.5
(0.49)
(0.35)
Time (s)

Figure 4.4(b)

Figure 4.4. Dynamic stress caused by the surface waves generated by the DFE on the focal mechanisms triggered by the DFE (a) and on the focal mechanisms triggered by the Landers earthquake (b). Left panels show the stress caused on the axial plane defined as 'plane 1' and right panes for axial 'plane 2'. From top to bottom, the upper panels shows the stress caused by the Love waves in the dip, strike and normal direction; stress caused by the Rayleigh waves in the dip, strike and normal direction, and the sum of these components for every direction labeled as 'total' (i.e.' $\delta\tau_s$ Total = $\delta\tau_s$ Love + $\delta\tau_s$ Rayleigh'). Numbers inside parentheses at the left of each panel represent the maximum stress (in MPa) reached for the corresponding component. Bottom panel shows the change in the Coulomb failure function or triggering potential as defined by equation 1 for normal faulting caused by the surface waves.

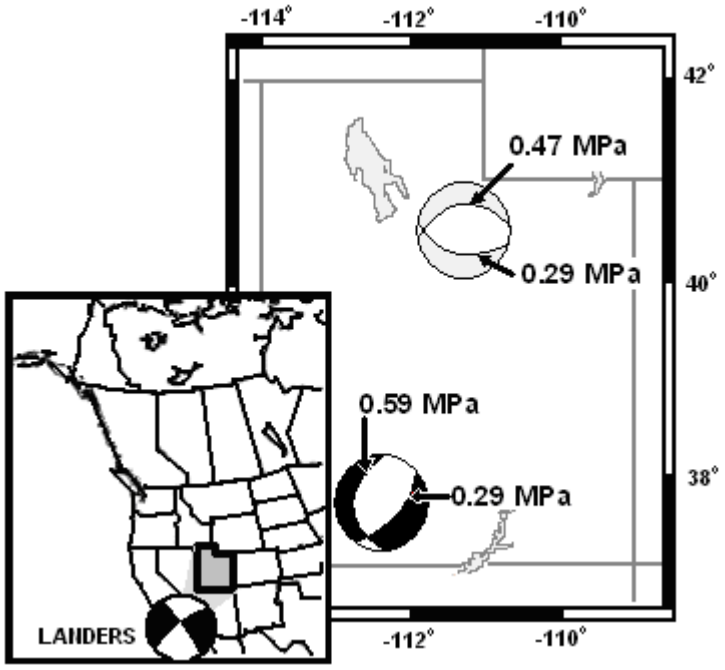

Figure 4.5. Black beach ball represents the earthquake triggered by the Landers event and gray color beach ball represents the earthquake triggered by the DFE. Triggering potentials for the surface waves generated by the Landers event, on the two possible axial planes, are shown for each focal mechanism.

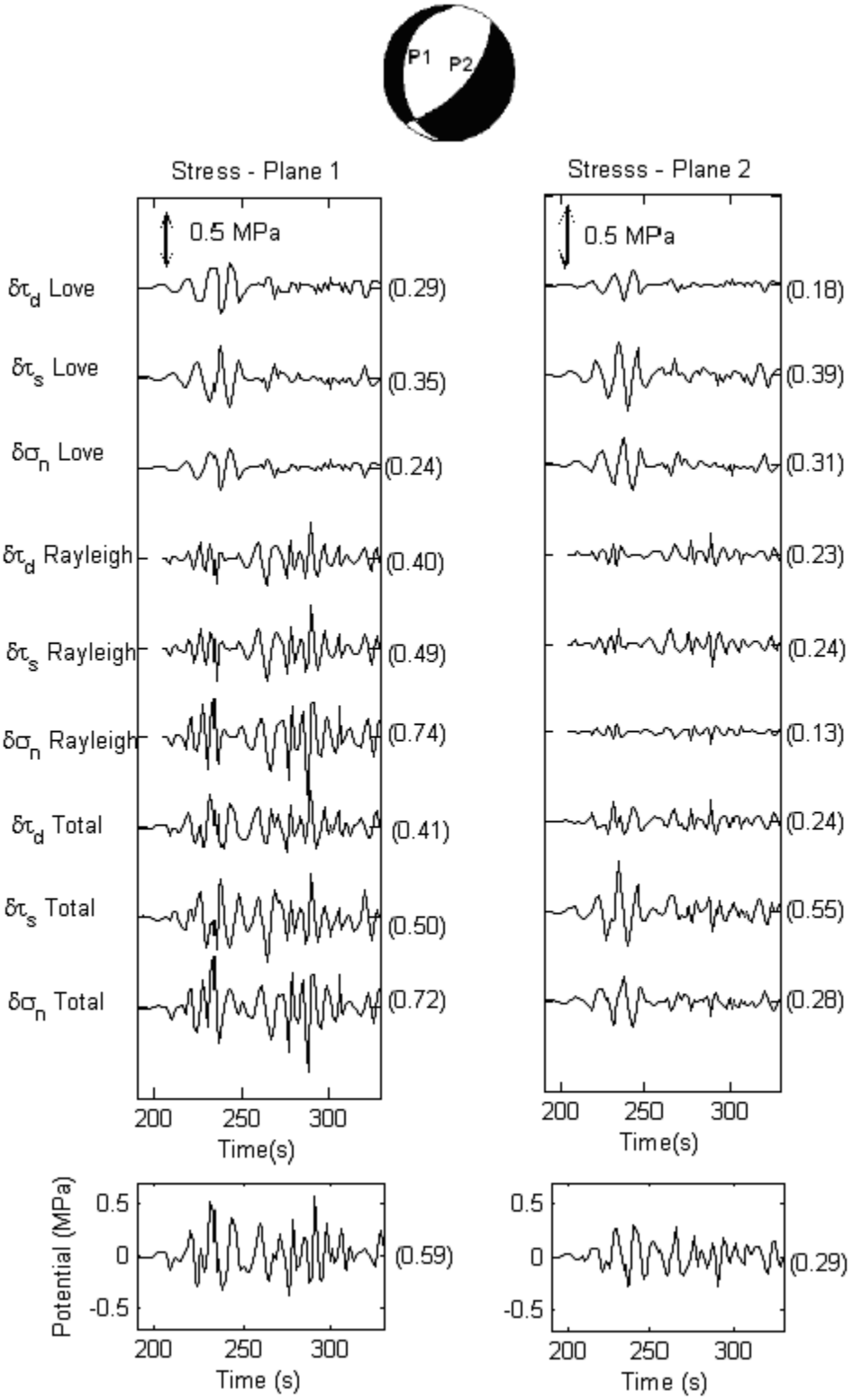
P1
P2
Stress - Plane 1
Stresss - Plane 2
0.5 MPa
0.5 MPa
δτd Love
δτs Love
δσn Love
δτd Rayleigh
δτs Rayleigh
δσn Rayleigh
δτd Total
δτs Total
δσn Total
(0.29)
(0.35)
(0.24)
(0.40)
(0.49)
(0.74)
(0.41)
(0.50)
(0.72)
(0.18)
(0.39)
(0.31)
(0.23)
(0.24)
(0.13)
(0.24)
(0.55)
(0.28)
200
250
300
Time(s)
Potential (MPa)
0.5
0
-0.5
(0.59)
(0.29)
Time (s)

Figure 4.6(a)

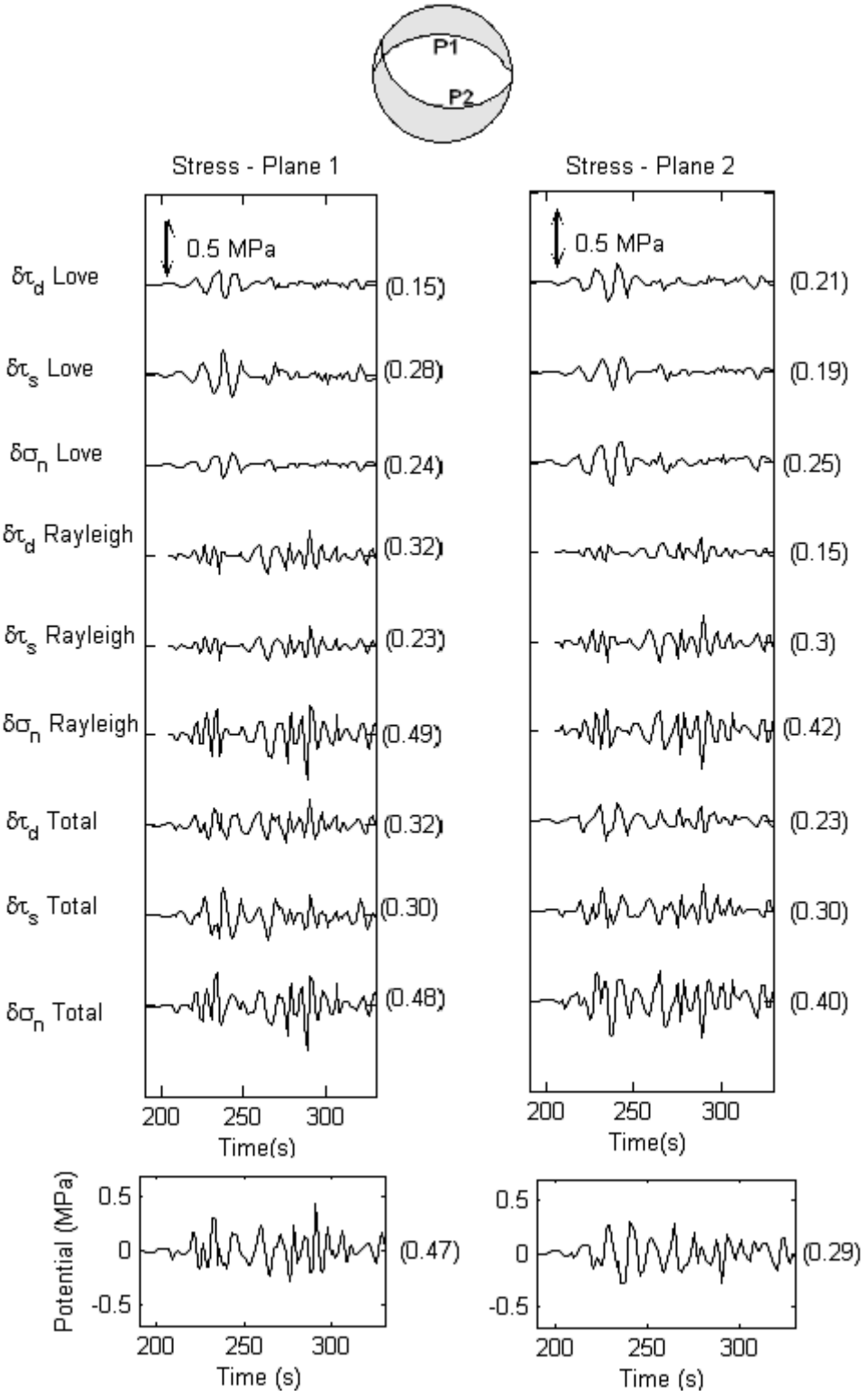
P1
P2
Stress - Plane 1
Stress - Plane 2
0.5 MPa
0.5 MPa
δτd Love
δτs Love
δσn Love
δτd Rayleigh
δτs Rayleigh
δσn Rayleigh
δτd Total
δτs Total
δσn Total
(0.15)
(0.28)
(0.24)
(0.32)
(0.23)
(0.49)
(0.32)
(0.30)
(0.48)
(0.21)
(0.19)
(0.25)
(0.15)
(0.3)
(0.42)
(0.23)
(0.30)
(0.40)
200 250 300
Time(s)
200 250 300
Time(s)
Potential (MPa)
0.5
0
-0.5
(0.47)
(0.29)
200 250 300
Time (s)
200 250 300
Time (s)

Figure 4.6(b)

Figure 4.6. Dynamic stress caused by the surface waves generated by the Landers event on the focal mechanisms triggered by the Landers (a) and on the focal mechanisms triggered by the DFE (b). Left panels show the stress caused on the axial plane defined as ‘plane 1’ and right panes for axial ‘plane 2’. See figure 4 for panels’ descriptions.

CURRICULUM VITA

Hector Gonzalez-Huizar was born in Zacatecas, Mexico. The third son of Herminio Gonzalez and Guadalupe Huizar, he graduated from the Miguel Agustin Pro high school and entered Universidad Autonoma de Zacatecas in 1997. He graduated with Bachelor degree in Physics and entered The University of Texas at El Paso (UTEP) in 2001 where he graduated with a Masters degree in Physics. He entered the Department of Geological Sciences at UTEP in 2004 to pursue a Doctoral degree in Geophysics where he worked as TA and RA. He was recipient of the NSF Graduate Teaching Fellowship in K-12 Education grant and of the Geological Society of America 2008 Research Grant.

Present Address Hector Gonzalez-Huizar

Geological Sciences Department-UTEP

El Paso, TX 79902